

Spontaneous Formation in the Dark, and Visible Light-Induced Cleavage, of a Ru–S Bond in Water: A Thermodynamic and Kinetic Study

Azadeh Bahreman,[†] Bart Limburg,[†] Maxime A. Siegler,[‡] Elisabeth Bouwman,[†] and Sylvestre Bonnet^{*,†}

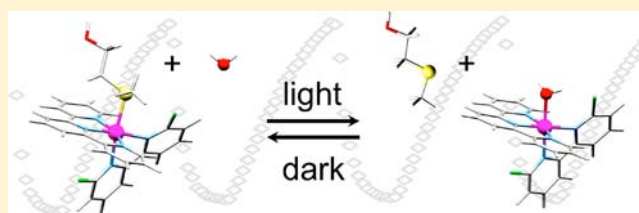
[†]Leiden Institute of Chemistry, Gorlaeus Laboratories, Leiden University, P.O. Box 9502, Leiden, 2300 RA, The Netherlands

[‡]Small Molecule X-ray Facility, Department of Chemistry, Johns Hopkins University, Baltimore, Maryland 21218, United States

Supporting Information

ABSTRACT: In this work the thermal and photochemical reactivity of a series of ruthenium complexes $[\text{Ru}(\text{terpy})(\text{N}-\text{N})(\text{L})](\text{X})_2$ (terpy = 2,2';6',2''-terpyridine, L = 2-(methylthio)ethanol (Hmte) or water, and X is Cl^- or PF_6^-) with four different bidentate chelates N–N = bpy (2,2'-bipyridine), biq (2,2'-biquinoline), dcbpy (6,6'-dichloro-2,2'-bipyridine), or dmbpy (6,6'-dimethyl-2,2'-bipyridine), is described. For each chelate N–N the thermodynamic constant

of the dark equilibrium between the aqua- and Hmte- complexes, the Hmte photosubstitution quantum yield, and the rate constants of the thermal interconversion between the aqua and Hmte complexes were measured at room temperature. By changing the steric hindrance and electronic properties of the spectator N–N ligand along the series bpy, biq, dcbpy, dmbpy the dark reactivity clearly shifts from a nonlabile equilibrium with N–N = bpy to a very labile thermal equilibrium with N–N = dmbpy. According to variable-temperature rate constant measurements in the dark near pH = 7 the activation enthalpies for the thermal substitution of H_2O by Hmte are comparable for all ruthenium complexes, whereas the activation entropies are negative for bpy and biq, and positive for dcbpy and dmbpy complexes. These data are indicative of a change in the substitution mechanism, being interchange associative with nonhindered or poorly hindered chelates (bpy, biq), and interchange dissociative for more bulky ligands (dcbpy, dmbpy). For the most labile dmbpy system, the thermal equilibrium is too fast to allow significant modification of the composition of the mixture using light, and for the nonhindered bpy complex the photosubstitution of Hmte by H_2O is possible but thermal binding of Hmte to the aqua complex does not occur at room temperature. By contrast, with N–N = biq or dcbpy the thermodynamic and kinetic parameters describing the formation and breakage of the Ru–S bond lie in a range where the bond forms spontaneously in the dark, but is efficiently cleaved under light irradiation. Thus, the ratio between the aqua and Hmte complex in solution can be efficiently controlled at room temperature using visible light irradiation.



INTRODUCTION

Visible light is an efficient tool to control molecular and supramolecular metal-based systems,^{1–10} for applications in material science,^{11–14} nanotechnologies,^{15–25} or medicine.^{26–45} Among the vast family of photosensitive compounds ruthenium(II) polypyridyl complexes certainly play a prominent role.^{18,46} Whereas $[\text{Ru}(\text{bpy})_3]^{2+}$ -type complexes are notorious for their luminescence,^{47–50} complexes bearing terpyridyl-like ligands, or sterically hindered chelates, have emerged for their ability to selectively photosubstitute one of the ligands of the coordination sphere by solvent molecule(s).^{25,49,51–54} Such reactivity is based on low-lying, metal-centered (³MC) excited states with dissociative character that are thermally populated from the photochemically generated metal-to-ligand charge-transfer (³MLCT) excited states. In such systems, the photosubstitution reaction can be used to power a molecular machine^{20,23,24,55–60} or trigger molecular switches.^{12–14,61} More recently, visible light-induced photosubstitution reactions have been proposed as a new way to

activate “caged” bioactive ruthenium complexes or ligands.^{29,33,36,38,43,62}

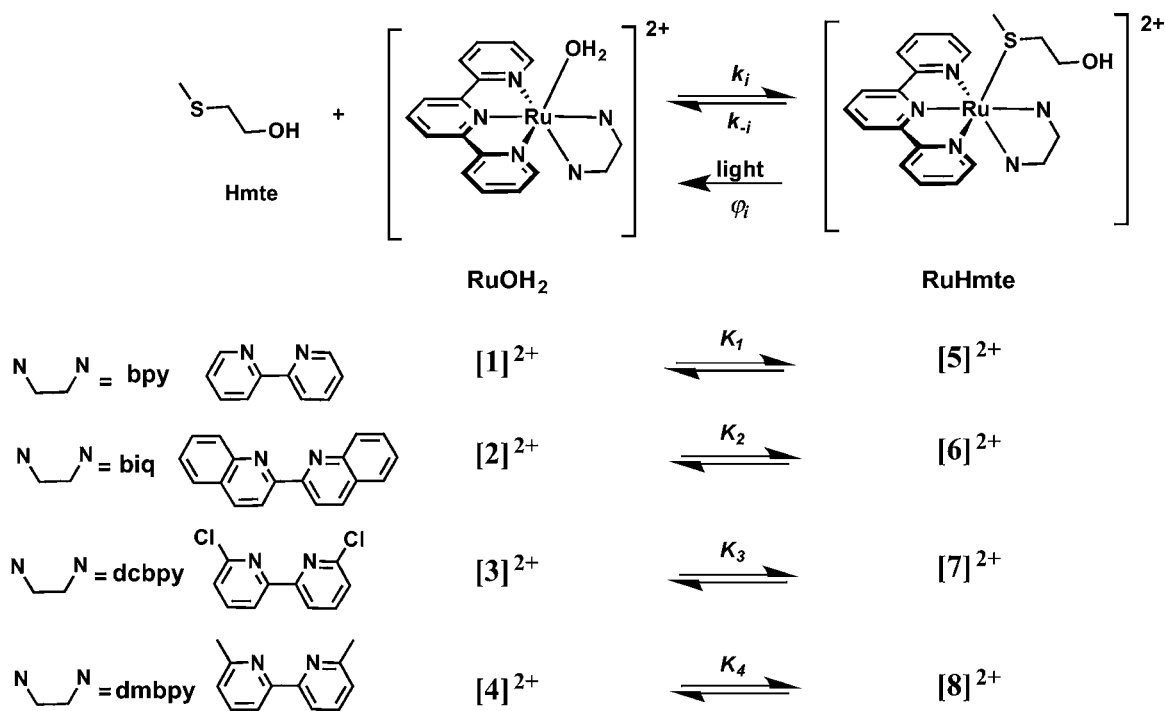
It has been clearly demonstrated, notably by Sauvage et al., that in solution the steric properties of the spectator ligands influence dramatically the quantum efficiency of photosubstitution reactions.^{24,63} This phenomenon is interpreted as a cause of the distortion of the coordination octahedron induced by steric bulkiness, which in turn lowers the ligand field splitting energy of the complex and brings the ³MC states closer in energy to the photogenerated ³MLCT states. However, the electronic and steric properties of the ligand set also influence the thermal reactivity of the metal complex. In principle, the thermal coordination of sterically hindered ligands requires more thermal energy than that of unhindered ligands.²⁴ Two decades ago however, Takeuchi et al. reported the reverse phenomenon in a family of complexes $[\text{Ru}(\text{terpy})(\text{N}-\text{N})(\text{L})]^{2+}$ (terpy = 2,2';6',2''-terpyridine, L = H_2O or

Received: May 3, 2013

Published: August 2, 2013

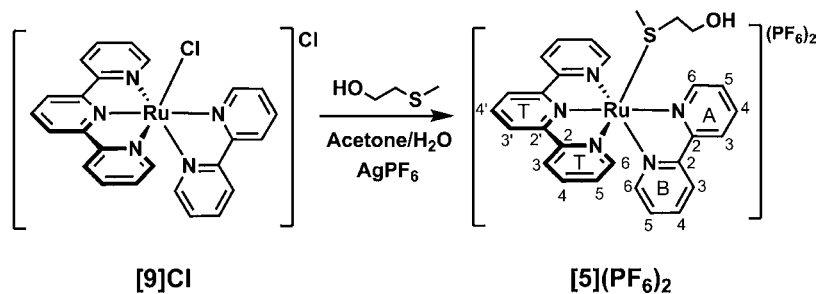


Scheme 1. Thermal Equilibrium between $[\text{Ru}(\text{terpy})(\text{N}-\text{N})(\text{OH}_2)]^{2+}$ and $[\text{Ru}(\text{terpy})(\text{N}-\text{N})(\text{Hmte})]^{2+}$, and the Photosubstitution of Hmte by an Aqua Ligand^a



^a k_i are second-order rate constants for the thermal substitution of H_2O by Hmte (unit: $\text{M}^{-1} \text{s}^{-1}$), k_{i-1} are first-order rate constants for the thermal substitution of Hmte by H_2O (unit: s^{-1}), K_i the thermodynamic equilibrium constants (unit: M^{-1}), and ϕ_i are the photosubstitution quantum yields (dimensionless). Indexes i refer to the complexes with $\text{N}-\text{N} = \text{bpy}$ ($i = 1$), $\text{N}-\text{N} = \text{biq}$ ($i = 2$), $\text{N}-\text{N} = \text{dcbpy}$ ($i = 3$), and $\text{N}-\text{N} = \text{dmbpy}$ ($i = 4$).

Scheme 2. Synthesis and Numbering Scheme of $[\text{Ru}(\text{terpy})(\text{bpy})(\text{Hmte})](\text{PF}_6)_2$ ($[5](\text{PF}_6)_2$)



CH_3CN), where the rate of the thermal substitution of the aqua ligand by acetonitrile at room temperature was increased with more sterically hindered spectator diimine ligands $\text{N}-\text{N}$.⁶⁴ This work introduced a quantitative measure of the steric bulkiness of diimine chelates, but it remained elusive on the reasons for the higher lability of the aqua ligand observed with hindered spectator chelates. The reaction was studied at a single temperature, and based on earlier work⁶⁵ a dissociative-interchange substitution mechanism was proposed without variable-temperature kinetic measurements.

Inspired by these results we recently studied the substitution reaction of $[\text{Ru}(\text{terpy})(\text{dcbpy})(\text{OH}_2)]^{2+}$ ($\text{dcbpy} = 6,6'$ -dichloro-2,2'-bipyridine) with 2-methylthioethanol (hereafter, Hmte) in pure water. At room temperature, binding of the thioether ligand to afford $[\text{Ru}(\text{terpy})(\text{dcbpy})(\text{Hmte})]^{2+}$ is a fast reaction.²² We realized that considering the high photosubstitution quantum yield of the Hmte complex (0.13 at 465 nm) to afford the starting aqua complex $[\text{Ru}(\text{terpy})(\text{dcbpy})(\text{OH}_2)]^{2+}$, this system represented a very interesting tool in supramolecular chemistry, as the chemical equilibrium

between the aqua and the Hmte ruthenium complexes can be shifted by visible light, while re-establishing itself in the dark. We now broaden this work by studying in water the thermal coordination of Hmte to $[\text{Ru}(\text{terpy})(\text{N}-\text{N})(\text{OH}_2)]^{2+}$ (hereafter, RuOH_2) with a series of three bidentate ligands having different steric demands, namely $\text{N}-\text{N} = \text{bpy}$ (2,2'-bipyridine), biq (2,2'-biquinoline), or dmbpy (6,6'-dimethyl-2,2'-bipyridine, see Scheme 1). The aim of the present work was double: first, we wanted to obtain a complete overview of the effect of sterically hindered substituents on the thermal and photochemical reactivity of $\text{Ru}(\text{II})$ complexes in water (Scheme 1). Second, we aimed at unraveling the mechanism of the thermal coordination of Hmte to the aqua complex, and to understand the counterintuitive observation that ligand binding to more hindered complexes is faster. We demonstrate here that the higher thermal lability of the hindered complexes is due to a change in the ligand substitution mechanism, from interchange associative with the nonhindered bpy $\text{N}-\text{N}$ chelate, to interchange dissociative with the most hindered dcbpy and dmbpy complexes.

RESULTS

Synthesis and Crystal Structure. The new complex $[\text{Ru}(\text{terpy})(\text{bpy})(\text{Hmte})](\text{PF}_6)_2$ ($[\mathbf{5}](\text{PF}_6)_2$) was synthesized by silver-induced removal of the chloride ligand of $[\text{Ru}(\text{terpy})(\text{bpy})\text{Cl}]\text{Cl}$ ($[\mathbf{9}]\text{Cl}$) in presence of Hmte at elevated temperatures (see Scheme 2). $[\mathbf{5}](\text{PF}_6)_2$ was characterized by ^1H NMR and ^{13}C NMR spectroscopy (Supporting Information, Figure S2), electrospray mass spectrometry (ES-MS), elemental analysis, and electron absorption spectroscopy (UV-vis). ^1H NMR spectroscopy in acetone- d_6 showed that the protons of the Hmte ligand (3.55 ppm, 2.00 ppm, 1.53 ppm) are shielded in $[\mathbf{5}](\text{PF}_6)_2$ compared to free Hmte (3.89 ppm, 2.58 ppm, 2.07 ppm) because of coordination to the ruthenium polypyridyl complex. Single crystals of $[\mathbf{5}](\text{PF}_6)_2$ were obtained by slow vapor diffusion of toluene into a solution of $[\mathbf{5}](\text{PF}_6)_2$ in Hmte. The crystal structure of the complex was determined by single-crystal X-ray diffraction (see Figure 1). As expected,

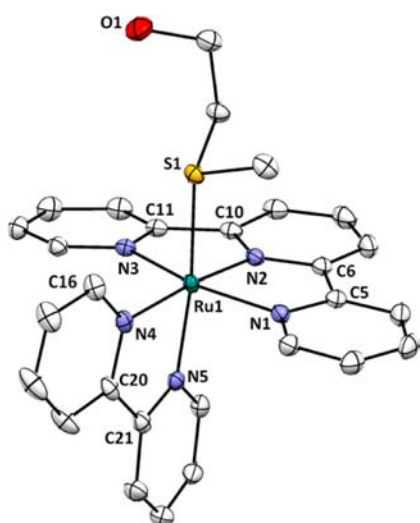


Figure 1. Displacement ellipsoid plot (at 50% probability level) of complex $[\mathbf{5}](\text{PF}_6)_2$. Hexafluorophosphate counterions and H atoms were omitted for clarity.

the Hmte ligand is coordinated to ruthenium(II) via its soft sulfur atom. The bpy ligand in $[\mathbf{5}](\text{PF}_6)_2$ is positioned almost perpendicular to the terpy. The comparison of the crystal structure of $[\mathbf{5}](\text{PF}_6)_2$ to that of the previously reported complex $[\text{Ru}(\text{terpy})(\text{dcbpy})(\text{Hmte})](\text{PF}_6)_2$ ($[\mathbf{7}](\text{PF}_6)_2$),²² shows that the torsion angles Ru1–N4–C20–C21 and Ru1–N5–C21–C20 for the bpy derivative are much smaller than those of the dcbpy derivative (see Table 1), which suggests that the coordination sphere is less distorted in $[\mathbf{5}](\text{PF}_6)_2$. Moreover, the Ru1–S1 bond in $[\mathbf{5}](\text{PF}_6)_2$ is slightly shorter (2.3690(5) Å) than that in $[\mathbf{7}](\text{PF}_6)_2$ (2.3819(6) Å, see Table 1), also indicating less steric hindrance in $[\mathbf{5}](\text{PF}_6)_2$. These results are similar to those reported for $[\text{Ru}(\text{terpy}^*)(\text{phen})(\text{dms})](\text{PF}_6)_2$ and $[\text{Ru}(\text{terpy}^*)(\text{dmp})(\text{dms})](\text{PF}_6)_2$ (terpy* = 4'-(3,5-dit-butylphenyl)-2,2';6';2"-terpyridine, phen = 1,10-phenanthroline, dmp = 2,9-dimethyl-1,10-phenanthroline, and dms = dimethyl sulfide).⁶³

Unlike $[\mathbf{5}](\text{PF}_6)_2$ and $[\mathbf{7}](\text{PF}_6)_2$,²² the RuHmte complexes $[\text{Ru}(\text{terpy})(\text{biq})(\text{Hmte})](\text{PF}_6)_2$ ($[\mathbf{6}](\text{PF}_6)_2$) and $[\text{Ru}(\text{terpy})(\text{dmbpy})(\text{Hmte})](\text{PF}_6)_2$ ($[\mathbf{8}](\text{PF}_6)_2$) could not be isolated in the solid state. Mixing $[\text{Ru}(\text{terpy})(\text{biq})(\text{Cl})]\text{Cl}$ ($[\mathbf{10}]\text{Cl}$) or $[\text{Ru}(\text{terpy})(\text{dmbpy})(\text{Cl})]\text{Cl}$ ($[\mathbf{12}]\text{Cl}$), respectively, with AgPF_6

Table 1. Selected Bond Lengths (Å) and Angles (deg) for $[\mathbf{5}](\text{PF}_6)_2$ and $[\mathbf{7}](\text{PF}_6)_2$ ²²

	$[\mathbf{5}](\text{PF}_6)_2^a$	$[\mathbf{7}](\text{PF}_6)_2^b$
Ru1–S1	2.3690(5)	2.3819(6)
Ru1–N1	2.061(1)	2.084(2)
Ru1–N2	1.961(1)	1.962(2)
Ru1–N3	2.066(1)	2.074(2)
Ru1–N4	2.092(1)	2.126(2)
Ru1–N5	2.064(1)	2.115(2)
Ru1–N4–C20–C21	2.3(2)	21.5(3)
Ru1–N5–C21–C20	10.5(2)	22.0(3)
Ru1–N1–C5–C6	1.8(2)	2.4(3)
Ru1–N3–C11–C10	5.0(2)	7.6(3)
Ru1–N2–C6–C5	2.7(2)	4.9(3)
Ru1–N2–C10–C11	2.8(2)	0.7(3)

^aThis work. ^bTaken from reference 22.

and Hmte in water, was followed by precipitation, but the resulting salts $[\mathbf{6}](\text{PF}_6)_2$ and $[\mathbf{8}](\text{PF}_6)_2$ were always impure after chromatography. Preparation of $[\mathbf{6}]^{2+}$ and $[\mathbf{8}]^{2+}$ in aqueous solution is straightforward, however, as they spontaneously and quantitatively form upon mixing $[\mathbf{10}]\text{Cl}$ or $[\mathbf{12}]\text{Cl}$ and an excess of Hmte in pure water, thus without addition of AgPF_6 . According to ^1H NMR in such conditions $[\mathbf{6}]^{2+}$ or $[\mathbf{8}]^{2+}$ are the only ruthenium species present in solution (see Figure 2 and Supporting Information, Figure S3). Both complexes were fully characterized in solution by ^1H and ^{13}C NMR, electrospray mass spectrometry, and UV-vis spectroscopy (see Experimental Part).

Dissolution of the nonhindered bpy complex $[\mathbf{9}]\text{Cl}$ in water notoriously leads to a slow equilibrium between the chlorido complex $[\mathbf{9}]^+$ and the aqua complex $[\text{Ru}(\text{terpy})(\text{bpy})(\text{OH}_2)]^{2+}$ ($[\mathbf{1}]^{2+}$).^{33,66} This equilibrium establishes within hours at room temperature. By contrast, the chlorido complexes $[\mathbf{10}]\text{Cl}$ or $[\mathbf{12}]\text{Cl}$ are, within minutes at room temperature, fully hydrolyzed into the aqua species $[\mathbf{2}]^{2+}$ or $[\mathbf{4}]^{2+}$, respectively. Indeed, according to ^1H NMR adding increasing amount of D_2O to CD_3OD solutions of $[\mathbf{10}]\text{Cl}$ or $[\mathbf{12}]\text{Cl}$ leads, within the time necessary for recording a ^1H NMR spectrum, to the formation of a second species (see Supporting Information, Figure S4). In pure D_2O , the ^1H NMR spectrum of $[\mathbf{10}]\text{Cl}$ or $[\mathbf{12}]\text{Cl}$ shows a unique A8 or A5 doublet at 6.75 ppm or 6.78 ppm (see Figure 2 and Supporting Information, Figure S1), respectively. Aqua Ru(II) complexes are very weak acids in water, with typical $\text{p}K_a$ values above 9.5. The $\text{p}K_a$ of $[\mathbf{2}]^{2+}$ and $[\mathbf{4}]^{2+}$ were unknown; UV-vis titration led to values of 9.5 and 10.5, respectively (see Supporting Information, Figure S5), which is comparable to that of $[\mathbf{1}]^{2+}$ (9.7) and $[\mathbf{3}]^{2+}$ (10.9).^{67,68} As a consequence, complexes $[\mathbf{1}]^{2+}$ – $[\mathbf{4}]^{2+}$ are not deprotonated in pure water near pH 7, and dissolving in Milli-Q water $[\mathbf{10}]\text{Cl}$ or $[\mathbf{12}]\text{Cl}$ produces only the aqua complex $[\mathbf{2}]^{2+}$ or $[\mathbf{4}]^{2+}$, respectively. We recently published a similar observation for the dcbpy system.²² Thus, the hydrolysis of the Ru–Cl bond in water is fast at room temperature with hindered N–N ligands (biq, dmbpy, or dcbpy), and the hindered chlorido compounds are good precursors for the corresponding aqua complexes in nonbasic solutions.

As noted above, with hindered complexes (N–N = biq, dmbpy, or dcbpy²²), addition of an excess of Hmte to a solution of the chlorido precursor complex $[\text{Ru}(\text{terpy})(\text{N–N})\text{Cl}]\text{Cl}$ (hereafter noted $[\text{RuCl}]\text{Cl}$) in pure water leads, in the dark and at room temperature, to an equilibrium between the

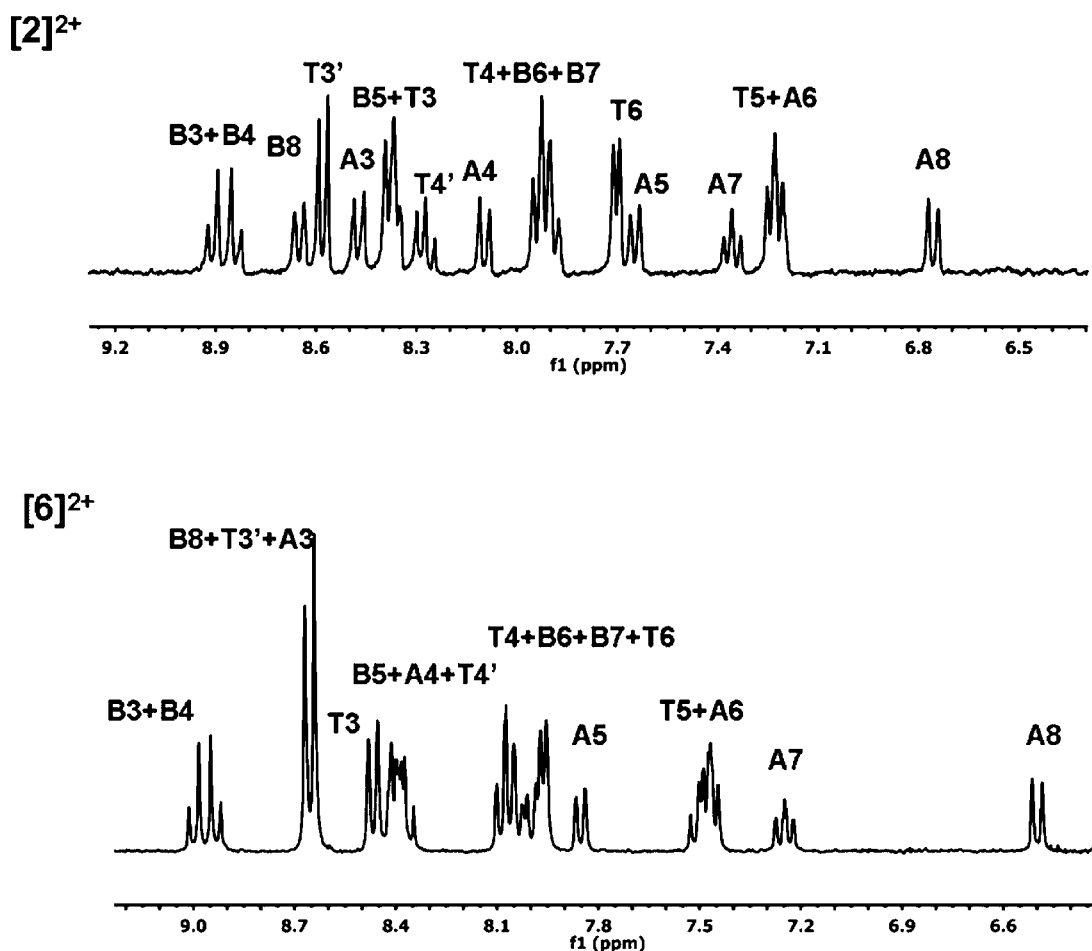


Figure 2. ^1H NMR of a solution of $[2]^{2+}$ (top) and $[6]^{2+}$ (down) in pure D_2O near pH 7 (aromatic region, N–N = biq). Conditions: $[\text{Ru}]_{\text{tot}} = 12$ mM, $[\text{Hmte}] = 0$ (top) or 0.93 M (bottom), MilliQ water (pH ~ 7), 298 K. See Supporting Information, Figure S1 for proton attributions.

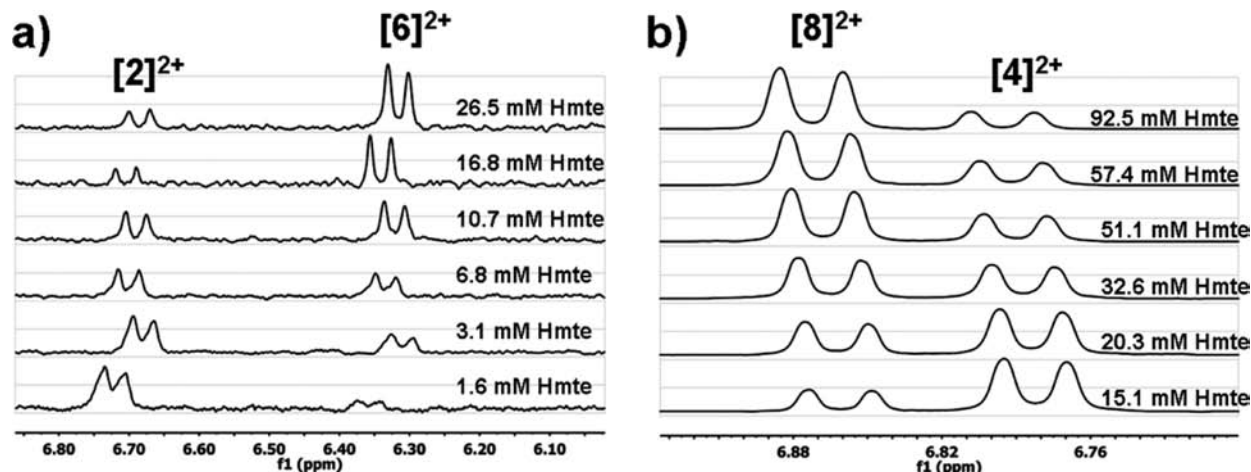


Figure 3. Evolution of the ^1H NMR spectra, at the equilibrium between RuOH_2 and RuHmte , with different initial concentrations of Hmte for (a) the equilibrium between $[2]^{2+}$ and $[6]^{2+}$ (N–N = biq); (b) the equilibrium between $[4]^{2+}$ and $[8]^{2+}$ (N–N = dmbpy). Condition: (a) $[\text{Ru}]_{\text{tot}} = 5.13$ mM, (b) $[\text{Ru}]_{\text{tot}} = 12.7$ mM, in D_2O , pH ~ 7 (pure water), $T = 297$ K, in the dark. The initial amounts of Hmte are indicated on each spectrum.

corresponding aqua species $[\text{Ru}(\text{terpy})(\text{N}-\text{N})(\text{OH}_2)]^{2+}$ ($[2]^{2+}$ – $[4]^{2+}$, noted RuOH_2) and the S-bonded Hmte ruthenium complexes $[\text{Ru}(\text{terpy})(\text{N}-\text{N})(\text{Hmte})]^{2+}$ ($[6]^{2+}$ – $[8]^{2+}$, noted RuHmte). Thioether ligands are not basic and, unlike for amine or pyridine ligands where a buffer is required, here the addition of even large excesses of Hmte to solutions of the aqua complex $[2]^{2+}$ – $[4]^{2+}$ does not lead to significant

deviations of the pH from 7. This was also observed upon adding Hmte to $[1]^{2+}$, which can be introduced in solution in the form of $[1](\text{PF}_6)_2$. Typically, in presence of 0.1 M Hmte a 10^{-4} M solution of $[1](\text{PF}_6)_2$, $[10]\text{Cl}$, $[11]\text{Cl}$, or $[12]\text{Cl}$ in Milli-Q water has a pH of 7.2–7.4, that is, the aqua complex $[1]^{2+}$, $[2]^{2+}$, $[3]^{2+}$, or $[4]^{2+}$ is not deprotonated. The substitution of the aqua ligand in $[1]^{2+}$ by Hmte can be

studied above 50 °C, whereas for the hindered biq, dcbpy, and dmbpy system it was studied at room temperature and above (see below). The overall equilibria for the four systems are summarized in Scheme 1.

Thermodynamic Study. ^1H NMR experiments were performed in D_2O to measure the equilibrium constants K_2 and K_4 for the equilibria between $[\text{2}]^{2+}$ and $[\text{6}]^{2+}$ (N–N = biq), and between $[\text{4}]^{2+}$ and $[\text{8}]^{2+}$ (N–N = dmbpy), respectively (see Scheme 1). For each reaction, NMR samples containing the RuCl precursor $[\text{10}]\text{Cl}$ or $[\text{12}]\text{Cl}$ and different initial amounts of free Hmte were prepared. After equilibration at 24 °C in the dark, the ^1H NMR spectrum of each sample was measured. Integration of the two A8 doublets at 6.35 ($[\text{6}]^{2+}$) and 6.75 ($[\text{2}]^{2+}$) ppm (N–N = biq), or of the two A5 doublets at 6.86 ($[\text{8}]^{2+}$) and 6.78 ($[\text{4}]^{2+}$) ppm (N–N = dmbpy), allowed for calculating the relative amount of RuHmte and RuOH_2 present in solution (see Figure 3 and Supporting Information, Figure S1). A plot of the ratio $[\text{RuHmte}]/[\text{RuOH}_2]$ vs $[\text{Hmte}]$ is shown in Figure 4, where $[\text{RuHmte}]$, $[\text{RuOH}_2]$, and $[\text{Hmte}]$

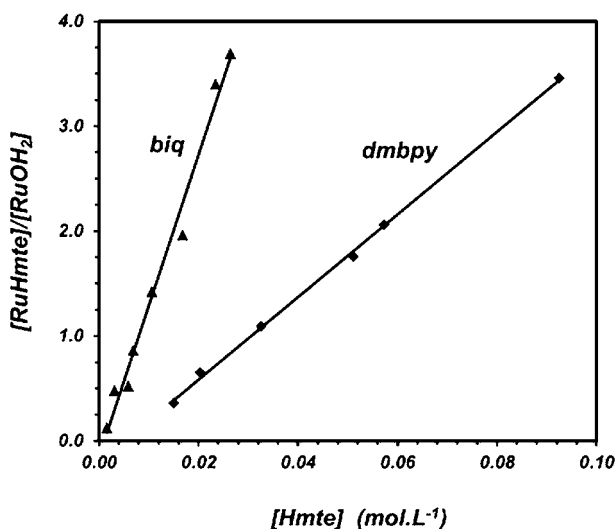


Figure 4. Plots of the ratio $[\text{RuHmte}]/[\text{RuOH}_2]$ at the equilibrium at 297 K, as a function of the equilibrium concentration in free Hmte. $[\text{RuHmte}]$ and $[\text{RuOH}_2]$ represents the concentrations (in mol L^{-1}) in $[\text{6}]^{2+}$ and $[\text{2}]^{2+}$, respectively (N–N = biq), or in $[\text{8}]^{2+}$ and $[\text{4}]^{2+}$, respectively (N–N = dmbpy).

represent the concentrations of the thioether complex, of the aqua complex, and of the free thioether ligand, respectively. For both reactions straight lines were obtained. According to eq 1 the slope of each line corresponds to the thermodynamic equilibrium constant K_2 (N–N = biq) and K_4 (N–N =

dmbpy); the values were found to be $143(10) \text{ M}^{-1}$ and $37(2) \text{ M}^{-1}$, respectively, at 297 K, in pure water and in the dark. These values are both slightly lower than that of the dcbpy system ($K_3 = 151(8) \text{ M}^{-1}$ in the same conditions,²² see Table 2).

$$\frac{[\text{RuHmte}]}{[\text{RuOH}_2]} = K_i \cdot [\text{Hmte}] \quad (1)$$

Knowing the equilibrium constant for each reaction and using $\Delta G_i^\circ = -RT \cdot \ln(K_i)$, the free Gibbs energies ΔG_2° , ΔG_3° , and ΔG_4° were calculated at 297 K to be $-12(2) \text{ kJ mol}^{-1}$, $-13(2) \text{ kJ mol}^{-1}$, and $-9(1) \text{ kJ mol}^{-1}$, respectively, showing a lower thermodynamic driving force toward the formation of RuHmte for the most hindered dmbpy system, in water and at room temperature (see Table 3). The establishment of the

Table 3. Activation Parameters for the Thermal Coordination of Hmte to RuOH_2 (i) and Thermal Hydrolysis of RuHmte ($-i$)^a

N–N	ΔH_i^\ddagger ($\text{kJ}\cdot\text{mol}^{-1}$)	ΔS_i^\ddagger ($\text{J}\cdot\text{mol}^{-1}\cdot\text{K}^{-1}$)	ΔG_i^\ddagger (297 K) ($\text{kJ}\cdot\text{mol}^{-1}$)	ΔG_{-i}^\ddagger (297 K) ($\text{kJ}\cdot\text{mol}^{-1}$)	ΔG_i° (297 K) ($\text{kJ}\cdot\text{mol}^{-1}$)
bpy	83(1)	-48(9)	97(5)	117(20)	-20(2)
biq	79(3)	-20(8)	85(4)	97(6)	-12(2)
dcbpy	93(1)	+38(4)	82(3)	94(4)	-13(2)
dmbpy	85(1)	+20(2)	79(3)	88(4)	-9(1)

^aN–N is bpy ($i = 1$), biq ($i = 2$), dcbpy ($i = 3$), or dmbpy ($i = 4$). Condition: $T = 297 \text{ K}$, in the dark, Milli-Q water, $\text{pH} \sim 7$.

thermodynamic equilibrium for the unhindered N–N = bpy system is too slow at room temperature to be measured, and the corresponding equilibrium constant K_1 could not be obtained directly (see below).

Kinetic Study. Kinetic measurements were performed using UV–vis spectroscopy to compare the rate of the thermal substitution of the aqua ligand in $[\text{1}]^{2+}$, $[\text{2}]^{2+}$, and $[\text{4}]^{2+}$ by Hmte in pure water. After adding a large excess of Hmte to an aqueous solution of $[\text{10}]^+$ or $[\text{12}]^+$, the UV–vis spectrum of each solution with absorption maximum at 549 or 486 nm, respectively, gradually evolved within minutes in the dark to give rise to a new absorption maximum at 519 or 463 nm, corresponding to the Hmte complex $[\text{6}]^{2+}$ or $[\text{8}]^{2+}$, respectively. Clear isosbestic points (see Figures 5b and 5c) indicated a selective reaction involving only RuOH_2 and RuHmte. Remarkably, a solution of $[\text{1}]^{2+}$ containing large excess of the Hmte ligand is kinetically stable at room temperature, and coordination of the thioether ligand only takes place at temperatures above 323 K. At such high

Table 2. Thermodynamic and Kinetic Data at 297 K for the Interconversion between $[\text{Ru}(\text{terpy})(\text{N–N})(\text{OH}_2)]^{2+}$ and $[\text{Ru}(\text{terpy})(\text{N–N})(\text{Hmte})]^{2+}$ Complexes^a

i	N–N	K_i (M^{-1})	k_i ($\text{M}^{-1} \text{ s}^{-1}$)	$t_{1/2(i)}$ (min) ^d	k_{-i} (s^{-1})	$t_{1/2(-i)}$ (min)
1 ^b	bpy ^b	$6.8(8) \times 10^{+3}$	$1.5(9) \times 10^{-8}$	590(60)	$1.5(4) \times 10^{-8}$	$7.7(7) \times 10^{+5}$
2	biq	143(10)	$6.4(1) \times 10^{-3}$	9.0(9)	$4.5(9) \times 10^{-5}$	257(80)
3 ^c	dcbpy ^c	151(8)	$2.5(1) \times 10^{-2}$	2.3(1)	$1.6(9) \times 10^{-4}$	74(9)
4	dmbpy	37(2)	$1.2(5) \times 10^{-1}$	0.43(5)	$3.3(9) \times 10^{-3}$	6.5(5)

^aN–N is bpy, biq, dcbpy, and dmbpy. Conditions: in the dark, pure water, $\text{pH} \sim 7$. ^bData extrapolated at 297 K from the temperature-dependent kinetic measurements above 323 K (see text and Table 3). Uncertainties are high but the low rate constant obtained confirms the absence of measurable binding of Hmte to the unhindered aqua complex $[\text{1}]^{2+}$ at room temperature. ^cData taken from reference 22 for comparison. ^dCalculated for $[\text{Hmte}] = 0.2 \text{ M}$ ($t_{1/2(i)}$).

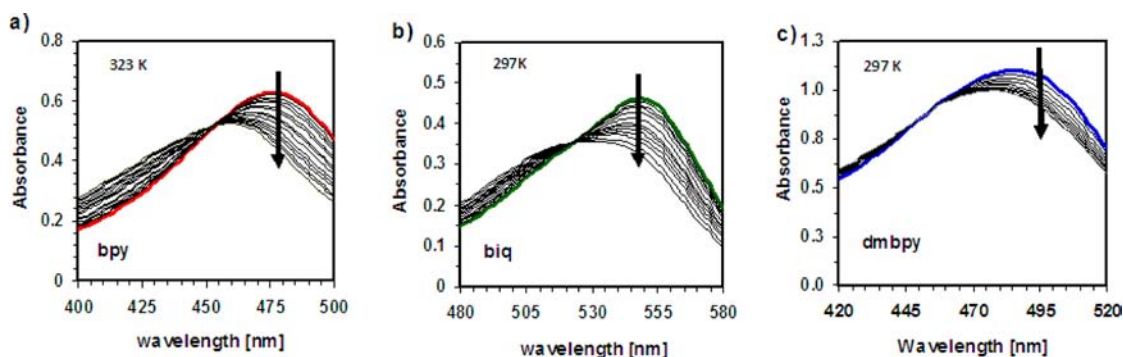


Figure 5. Time evolution of the UV-vis spectra of aqueous solutions initially containing (a) $[1]^{2+}$, (b) $[2]^{2+}$, and (c) $[4]^{2+}$, and a large excess of Hmte in Milli-Q water (pseudofirst order conditions). Conditions: (a) $T = 323$ K, $[\text{Ru}]_{\text{tot}} = 6.6 \times 10^{-5}$ M, $[\text{Hmte}] = 0.067$ M, (b) $T = 297$ K, $[\text{Ru}]_{\text{tot}} = 6.6 \times 10^{-5}$ M, $[\text{Hmte}] = 0.067$ M, and (c) $T = 297$ K, $[\text{Ru}]_{\text{tot}} = 2.1 \times 10^{-4}$ M, $[\text{Hmte}] = 0.032$ M.

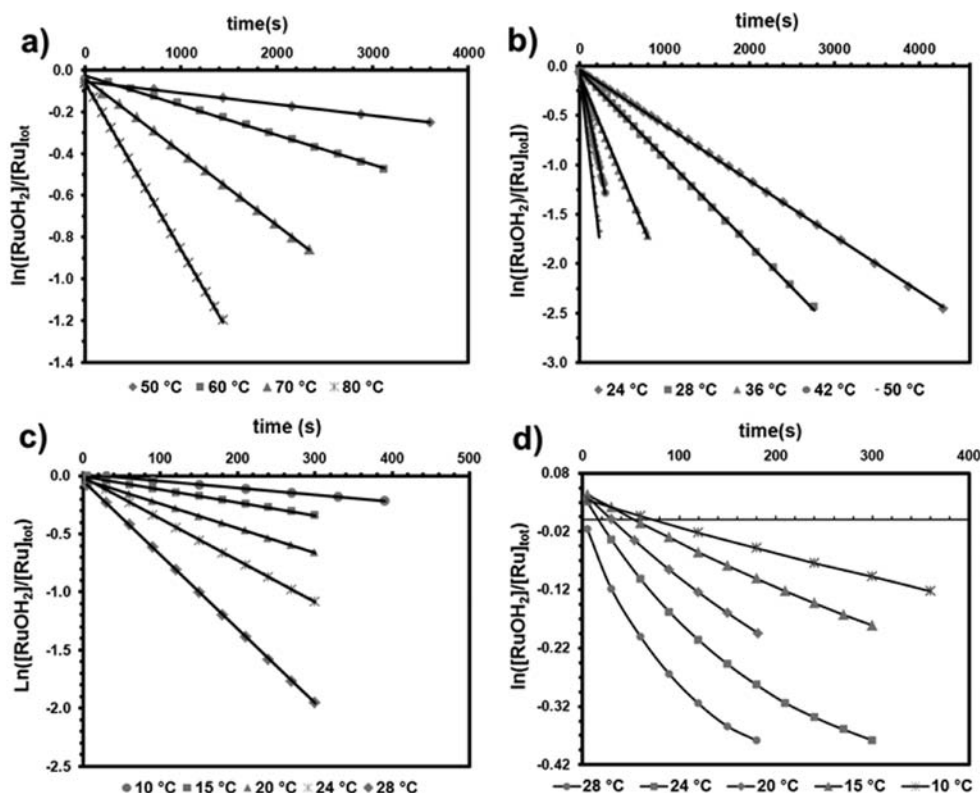


Figure 6. Plots of $\ln([\text{RuOH}_2]/[\text{Ru}]_{\text{tot}})$ vs time at different temperatures for the thermal coordination, in the dark and in pure water ($\text{pH} \sim 7$), of Hmte to (a) $[1]^{2+}$, (b) $[2]^{2+}$, (c) $[3]^{2+}$,²² and (d) $[4]^{2+}$. All the numerical values of k'_i and k_i are given in Supporting Information, Tables S2 and S3. Conditions: $T = 297$ K, (a) $[\text{Ru}]_{\text{tot}} = 6.6 \times 10^{-5}$ M, $[\text{Hmte}] = 0.067$ M, (b) $[\text{Ru}]_{\text{tot}} = 6.6 \times 10^{-5}$ M, $[\text{Hmte}] = 0.067$ M, (c) $[\text{Ru}]_{\text{tot}} = 1.4 \times 10^{-4}$ M, $[\text{Hmte}] = 0.16$ M, and (d) $[\text{Ru}]_{\text{tot}} = 2.1 \times 10^{-4}$ M, $[\text{Hmte}] = 0.032$ M.

temperatures, the Hmte complex $[5]^{2+}$ forms selectively, as shown by the clear isosbestic point at 455 nm and the final λ_{max} at 450 nm, which is identical to that of the isolated complex (see Figure 5a). For the two systems $\text{N}-\text{N} = \text{bpy}$ and biq the plots of $\ln([\text{RuOH}_2]/[\text{Ru}]_{\text{tot}})$ vs time were found linear at 323 and 297 K, respectively (Supporting Information, Figure S8), where $[\text{RuOH}_2]$ is the concentration in $[1]^{2+}$ or $[2]^{2+}$, and $[\text{Ru}]_{\text{tot}}$ is the total ruthenium concentration. The pseudo first-order rate constants k'_i ($i = 1$ or 2) were extracted from the slopes of these lines (see Figure 6), and a plot of k'_i vs $[\text{Hmte}]$ was found linear (Supporting Information, Figure S9), thus showing that the coordination of Hmte to $[1]^{2+}$ and $[2]^{2+}$ is first order in the ligand Hmte.

For $\text{N}-\text{N} = \text{dmbpy}$ the plot of $\ln([\text{RuOH}_2]/[\text{Ru}]_{\text{tot}})$ vs time at 297 K was not linear (see Figure 6d and Supporting Information, Figure S8) because with such a sterically hindered chelate the thermal back-substitution of Hmte by water cannot be neglected, that is, k_{-4} becomes comparable to k'_4 . Equation 2 and 3 give the general expression of the rate of the thermal formation of the RuHmte complex in pseudo first-order conditions. Equation 4 was obtained by integration, which was used to fit the plot $\ln([\text{RuOH}_2]/[\text{Ru}]_{\text{tot}})$ vs time and extract the values of $k_{\text{obs}} = k_{-4} + k'_4$ (see Supporting Information). Finally, a plot of k_{obs} vs $[\text{Hmte}]$ afforded a straight line, showing that also for $\text{N}-\text{N} = \text{dmbpy}$ the coordination of Hmte to $[4]^{2+}$ is first order in Hmte (see Supporting Information, Figure S9 for the full treatment).

Overall, like for $N-N = \text{dcbpy}^{22}$ the three rate laws for $N-N = \text{bpy}$, biq , and dmbpy were found to be first order in the Hmte ligand (see Supporting Information, Figures S8). The second-order rate constants k_i and the half-reaction time $t_{1/2(i)}$ (calculated with $[\text{Hmte}] = 0.2 \text{ M}$) are given in Table 2. At room temperature the $N-N = \text{biq}$ and $N-N = \text{dmbpy}$ systems are slower and faster, respectively, compared to the $N-N = \text{dcbpy}$ system. With $N-N = \text{bpy}$ Hmte does not coordinate to $[\mathbf{1}]^{2+}$ at 297 K, but k_1 and $t_{1/2(1)}$ can be measured at 323 K ($8.2(5) \times 10^{-4} \text{ M}^{-1} \text{ s}^{-1}$ and 71 min at $[\text{Hmte}] = 0.2 \text{ M}$, respectively). Even at such high temperatures the rate of the coordination reaction was found to be 8 times slower compared to the rate of the $N-N = \text{biq}$ system at 297 K (all other conditions being identical), which highlights the low lability of the nonhindered bpy system, compared to the sterically hindered ones.

$$\frac{d[\text{RuHmte}]}{dt} = k'_4[\text{RuOH}_2] - k_{-4}[\text{RuHmte}] \quad (2)$$

$$\frac{d[\text{RuHmte}]}{dt} = k'_4[\text{Ru}]_{\text{tot}} - [\text{RuHmte}](k'_4 + k_{-4}) \quad (3)$$

$$[\text{RuHmte}] = \frac{k'_4[\text{Ru}]_{\text{tot}}}{(k'_4 + k_{-4})} - \frac{c \cdot e^{-(k'_4 + k_{-4})t}}{(k'_4 + k_{-4})} \quad (4)$$

The pseudo first-order rate constants k_{-i} and half-reaction times $t_{1/2(-i)}$ for the thermal hydrolysis of the RuHmte complexes with $N-N = \text{biq}$, dcbpy , and dmbpy , in the dark and at 297 K, were determined from the knowledge of the thermodynamic equilibrium constants K_i , and the second-order rate constants k_i (see Table 2). Equation 5, written at the equilibrium, indeed rearranges into eq 6:

$$k_{-i} \cdot [\text{RuHmte}]_{\text{eq}} = k_i \cdot [\text{Hmte}]_{\text{eq}} \cdot [\text{RuOH}_2]_{\text{eq}} \quad (5)$$

$$k_{-i} = \frac{k_i}{K_i} \quad (6)$$

For the $N-N = \text{bpy}$ system measuring K_1 was not possible at room temperature and k_{-1} could not be calculated. However, k_{-1} could be obtained experimentally by heating an aqueous solution of $[\mathbf{5}](\text{PF}_6)_2$ at high temperatures ($>343 \text{ K}$), and monitoring by UV-vis spectroscopy the thermal substitution of Hmte by water at different temperatures. Subsequently, the activation parameters for the thermal hydrolysis of $[\mathbf{5}]^{2+}$ were extracted via an Eyring plot (see Supporting Information, Figure S10 and Table S4): values of $110(6) \text{ kJ mol}^{-1}$ and $-22(15) \text{ J mol}^{-1} \text{ K}^{-1}$ were found for ΔH_i^\ddagger and ΔS_i^\ddagger , respectively. By extrapolation of the values of k_{-1} at $T > 323 \text{ K}$, the value of ΔG_i^\ddagger and k_{-1} at 297 K were calculated to be $117(10) \text{ kJ mol}^{-1}$ and $1.5(9) \times 10^{-8} \text{ s}^{-1}$, respectively. The equilibrium constant K_1 at room temperature ($6.8(8) \times 10^{+3} \text{ M}^{-1}$) was obtained using eq 6 and the extrapolated value of k_1 at 297 K (see below and Table 2). These extrapolated values for $N-N = \text{bpy}$ are less precise than the direct measurements done for $N-N = \text{biq}$, dcbpy , and dmbpy considering the significant error on ΔS_i^\ddagger . However, they give a qualitative information about how *stable* and *inert* the nonhindered complex $[\mathbf{5}]^{2+}$ is. Finally, comparing the kinetic data in Table 2 shows that the thermal lability of both species RuOH_2 and RuHmte increases along the series bpy , biq , dcbpy , dmbpy , that is, upon increasing the steric hindrance of the spectator $N-N$ ligands. Such higher lability results in faster thermal

coordination, but also faster hydrolysis of the Hmte ligand, while the thermodynamic driving force for Hmte binding to ruthenium is lowered.

Activation Parameters for the Coordination of Hmte.

To obtain mechanistic information the rate of the thermal substitution of the aqua ligand by Hmte in $[\mathbf{1}]^{2+}$, $[\mathbf{2}]^{2+}$, $[\mathbf{3}]^{2+}$, or $[\mathbf{4}]^{2+}$ was studied at different temperatures using UV-vis spectroscopy. In pseudo first-order conditions the plot of $\ln([\text{RuOH}_2]/[\text{Ru}]_{\text{tot}})$ vs time at different temperatures afforded straight lines for $N-N = \text{bpy}$, biq , and dcbpy complexes (Figure 6a-c), which allowed determining the second-order rate constants k_i at different temperatures for all three reactions (Supporting Information, Table S3). For $N-N = \text{dmbpy}$ the $\ln([\text{RuOH}_2]/[\text{Ru}]_{\text{tot}})$ vs time data set was found non linear as explained above (Figure 6d). They were modeled using eq 4 and the values k_4 and k_{-4} could also be determined at five different temperatures (see Supporting Information, Table S2). The activation enthalpy ΔH_i^\ddagger , activation entropy ΔS_i^\ddagger , and activation Gibbs energy at 297 K, ΔG_i^\ddagger , are defined, for each reaction, by the Eyring equation (eq 7). In this equation k_i represents the second-order rate constant, k_B is the Boltzmann constant ($1.38 \times 10^{-23} \text{ J K}^{-1}$), h is Planck's constant ($6.63 \times 10^{-34} \text{ J s}$), and R is the gas constant ($8.314 \text{ J mol}^{-1} \text{ K}^{-1}$). An Eyring plot of $\ln(k_i/T)$ vs $1/T$ for the four systems afforded straight lines (see Figure 7), from which the values of ΔH_i^\ddagger and

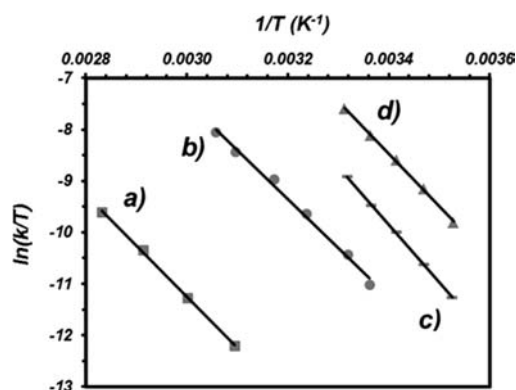


Figure 7. Eyring plots for the thermal substitution of H_2O by Hmte for $[\text{Ru}(\text{terpy})(N-N)(\text{OH}_2)]^{2+}$ in pure water, where $N-N$ is (a) bpy , (b) biq , (c) dcbpy , and (d) dmbpy . The slope of the line is $-\Delta H_i^\ddagger/R$, and the y-intercept is $\ln(k_i/h) + \Delta S_i^\ddagger/R$. See Table 3 for numerical values.

ΔS_i^\ddagger could be extracted. The activation Gibbs energies, ΔG_i^\ddagger , were calculated at 297 K using the equation $\Delta G_i^\ddagger = \Delta H_i^\ddagger - T\Delta S_i^\ddagger$ (see Table 3).

$$\ln \frac{k_i}{T} = \frac{-\Delta H_i^\ddagger}{R} \cdot \frac{1}{T} + \ln \frac{k_B}{h} + \frac{\Delta S_i^\ddagger}{R} \quad (7)$$

Quite surprisingly the four activation *enthalpies* were found too similar to account for the clear differences in reactivity between the four $N-N$ ligands. By contrast, unexpected differences in activation entropies were observed: the values for the less hindered $N-N = \text{bpy}$ and $N-N = \text{biq}$ bidentate ligands were found negative, whereas for the more hindering chelates $N-N = \text{dcbpy}$ and $N-N = \text{dmbpy}$ the values were found positive. When both contributions of enthalpy and entropy are taken into account, a clear trend was observed: the activation Gibbs energies ΔG_i^\ddagger decrease along the series bpy , biq , dcbpy , dmbpy . Such acceleration of the coordination of Hmte to the

Table 4. Photochemical and Thermal First-Order Rate Constant Values for a Typical Visible Light Irradiation Experiment with Interconversion between $[\text{Ru}(\text{terp})(\text{N}-\text{N})(\text{OH}_2)]^{2+}$ and $[\text{Ru}(\text{terpy})(\text{N}-\text{N})(\text{Hmte})]^{2+}$ ^a

N–N	[Hmte] (M)	k'_i (s ⁻¹)	k_{-i} (s ⁻¹)	$k_{\phi i}$ (s ⁻¹)	Φ (Einstein s ⁻¹)	ϕ_i
biq	0.011	7.3×10^{-5}	4.4×10^{-5}	4.2×10^{-4}	9.8×10^{-10}	0.12(5)
dc bpy	0.010	2.2×10^{-4}	1.1×10^{-4}	1.1×10^{-3}	3.9×10^{-9}	0.13(5)
dmbpy	0.20	1.8×10^{-2}	4.5×10^{-2}	2.0×10^{-3}	3.9×10^{-9}	0.30(6)

^a(N–N = biq, dc bpy, or dmbpy). Conditions: $T = 297$ K, solvent = Milli-Q water (pH ~ 7). The photon flux Φ is indicated.

aqua complex appears to be a consequence of a drastic increase of the activation entropy ΔS^\ddagger_i , that is, a change in the substitution mechanism, rather than a simple destabilization of RuOH_2 , which would lead to a decrease of the activation enthalpy ΔH^\ddagger_i (see discussion).

These variable-temperature measurements also allowed us to obtain the values of ΔG^\ddagger_{-i} for the thermal substitution of Hmte by water in $[\mathbf{6}]^{2+}$, $[\mathbf{7}]^{2+}$, or $[\mathbf{8}]^{2+}$, from the values of ΔG^\ddagger_i and ΔG°_i , and using the equation $\Delta G^\ddagger_{-i} = \Delta G^\ddagger_i - \Delta G^\circ_i$. Upon notably increasing the steric hindrance of the bidentate chelate, ΔG^\ddagger_{-i} was found to decrease as well (see Table 3), that is, the coordinated Hmte ligand becomes more and more labile in water. Overall, our data clearly indicate that increasing the bulkiness of the substituent on the bidentate chelate N–N increases the lability of both monodentate ligands (H_2O and Hmte), whereas it decreases the thermodynamic driving force for the formation of the RuHmte species.

Photochemistry. Quantum Yield Determination. Ruthenium polypyridyl complexes are known for their ability to photosubstitute a ligand of the coordination sphere by a solvent molecule upon visible light irradiation.^{20,21,25,46,51} The Ru–S bond of $[\mathbf{5}]^{2+}$, $[\mathbf{6}]^{2+}$, $[\mathbf{7}]^{2+}$, or $[\mathbf{8}]^{2+}$ can indeed be cleaved by visible light irradiation in water, to afford the ruthenium aqua complexes $[\mathbf{1}]^{2+}$, $[\mathbf{2}]^{2+}$, $[\mathbf{3}]^{2+}$, or $[\mathbf{4}]^{2+}$, respectively (see Scheme 1). This photochemical process comes in addition to the thermal hydrolysis of the Hmte complex, the kinetics of which significantly varies depending on the steric hindrance of the bidentate chelate N–N (see above and Table 2). Different methods were used for measuring the photosubstitution quantum yields ϕ_i of the four ruthenium compounds $[\mathbf{5}]^{2+}$ – $[\mathbf{8}]^{2+}$ (see Supporting Information). For $[\mathbf{5}]^{2+}$ full conversion to $[\mathbf{1}]^{2+}$ is obtained after 30 min irradiation at 452 nm using a 1000 W Xe lamp fitted with a bandpass filter. The photochemical reaction can be followed by UV–vis spectroscopy (Supporting Information, Figure S11), and a value of 0.022(6) was found for ϕ_1 at room temperature and at 452 nm, which is consistent with previous work.³³

On the other hand, measuring the photosubstitution quantum yields ϕ_2 , ϕ_3 , and ϕ_4 for $[\mathbf{6}]^{2+}$, $[\mathbf{7}]^{2+}$, and $[\mathbf{8}]^{2+}$, respectively, was challenging because of the rapid equilibrium between RuHmte and RuOH_2 .²² For these compounds standard measurements cannot be realized, so that another method was used consisting in the perturbation with light of the thermal equilibrium between RuOH_2 and RuHmte (see Supporting Information). In short, the ratio $[\text{RuHmte}]_{\text{eq}}/[\text{RuOH}_2]_{\text{eq}}$ is measured by UV–vis at the equilibrium in the dark (eq), and compared to the ratio $[\text{RuHmte}]_{\text{ss}}/[\text{RuOH}_2]_{\text{ss}}$ at the steady state under visible light irradiation (ss). Both ratios can be expressed as a function of k'_i , k_{-i} , and $k_{\phi i}$ (eq 8a and 8b), where $k_{\phi i}$ is a first-order rate constant for the photochemical substitution of Hmte by H_2O (unit: s⁻¹, see eq 9 and Supporting Information).

$$\begin{aligned} \text{(a)} \quad \frac{[\text{RuHmte}]_{\text{eq}}}{[\text{RuOH}_2]_{\text{eq}}} &= \frac{k_i[\text{Hmte}]}{k_{-i}} \\ \text{(b)} \quad \frac{[\text{RuHmte}]_{\text{ss}}}{[\text{RuOH}_2]_{\text{ss}}} &= \frac{k_i[\text{Hmte}]}{k_{-i} + k_{\phi i}} \end{aligned} \quad (8)$$

$$k_{\phi i} = \frac{\Phi \cdot \phi_i \cdot (1 - 10^{-A_i})}{n_{\text{Ru}(\text{tot})}} \quad (9)$$

First the value of k_i was obtained in the dark from eq 8(a) knowing the value of k_{-i} . Then the value of $k_{\phi i}$ can be obtained under irradiation using eq 8(b), and from the values of $k_{\phi i}$ the photosubstitution quantum yields ϕ_i were calculated using eq 9. Numerical values $\phi_2 = 0.12(5)$ (at 520 nm), $\phi_3 = 0.13(5)$ (at 465 nm), and $\phi_4 = 0.30(6)$ (at 465 nm) were found for the biq, dc bpy, and dmbpy systems, respectively, at 297 K. These values are significantly higher than ϕ_1 , as expected for sterically hindered complexes. The value of ϕ_3 found by this method was close to that obtained by us using a more direct method (0.097(9)).²²

Interestingly, comparing (Table 4) the pseudo first-order rate constant for the thermal substitution of H_2O by Hmte, k'_i , and the first-order rate constants k_{-i} and $k_{\phi i}$ for the thermal and photochemical substitution of Hmte by H_2O , respectively, highlights that with N–N = biq or N–N = dc bpy the values of $k_{\phi i}$ are 1 order of magnitude higher than that of k'_i and k_{-i} . In contrast, for N–N = dmbpy $k_{\phi 4}$ is 1 order of magnitude lower than k_{-4} and k'_{-4} . Thus, by increasing too much the steric hindrance of the spectator diimine bidentate ligand (N–N = dmbpy), the thermal lability of Hmte increases to a point where the light-induced shifting of the thermal equilibrium between RuOH_2 and RuHmte becomes difficult to realize. For such compounds shifting appreciably the equilibrium in favor of the aqua complex would require much higher light intensities. For N–N = biq and N–N = dc bpy low light intensities efficiently perturb the thermal equilibrium between RuOH_2 and RuHmte . As shown in Supporting Information, Figure S12b and S12c, during light irradiation the ratio $[\text{RuHmte}]/[\text{RuOH}_2]$ varies significantly: a steady state can be reached where Ru is mostly bound to H_2O , whereas in the dark it is mostly bound to Hmte. Thus, moderately hindered compounds such as those with biq and dc bpy represent a better compromise between thermal and photochemical lability, and afford a light-sensitive Ru–S coordination bond in water. By contrast, the thermal reactivity of nonhindered (N–N = bpy) or too hindered (N–N = dmbpy) complexes is either too low, or too high, respectively.

Reversibility of the Light-Induced Equilibrium Shift.

We recently showed that the blue light-induced shifting of the equilibrium between RuOH_2 and RuHmte in water for the N–N = dc bpy system could be repeated at least up to four cycles at room temperature.²² Considering the similar kinetic properties of the N–N = biq system, we repeated these studies for $[\mathbf{6}]^{2+}$ using green light. The thermal equilibrium between $[\mathbf{6}]^{2+}$ and

$[2]^{2+}$ in water was perturbed by light irradiation ($\lambda_e = 520$ nm) for a period of 45 min, followed by a dark period of 90 min. This cycle was repeated four times, and the state of the system was monitored by UV-vis spectroscopy. The time evolution of the ratio $[RuOH_2]/[Ru]_{tot}$ is shown in Figure 8. Like for N-N

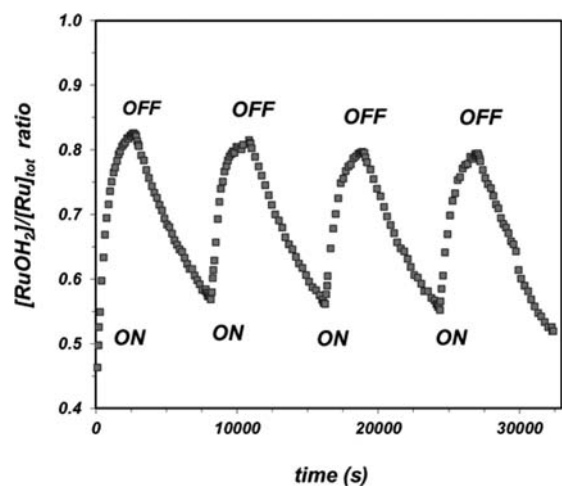


Figure 8. Plot of the ratio $[RuOH_2]/[Ru]_{tot}$ vs time upon switching ON and OFF several times a source of green light ($\lambda_e = 520$ nm) in presence of $[6]^{2+}$ and $[2]^{2+}$. Conditions: $T = 297$ K, Milli-Q water (pH ~ 7); photon flux $\Phi = 9.8(5) \times 10^{-9}$ Einstein s^{-1} ; $[Ru]_{tot} = 8.6 \times 10^{-5}$ M, $[Hmte] = 0.011$ M, spectra measured every 1 min.

= dcbpy, the N-N = biq system shows reversible light-induced shift of the equilibrium between $[6]^{2+}$ and $[2]^{2+}$, and no sign of degradation was observed after four cycles. The composition of the solution varies between 45% of $[2]^{2+}$ in the dark and up to 85% of $[2]^{2+}$ after irradiation. These results show that the biq

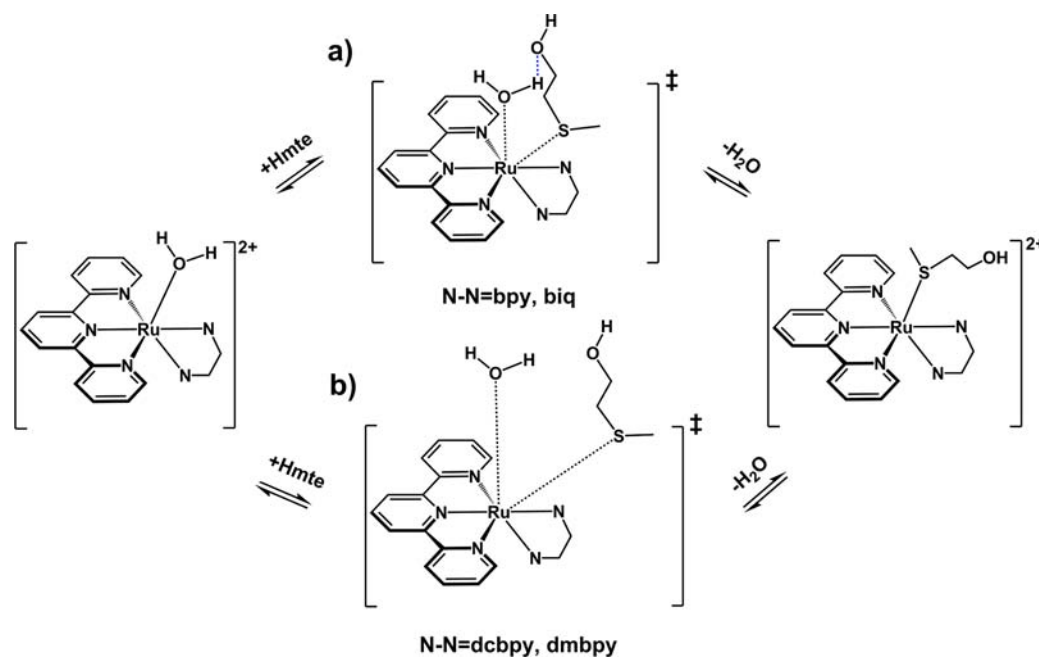
system is robust and only contains the two ruthenium complexes $[2]^{2+}$ and $[6]^{2+}$ that interconvert upon switching on and off a source of green light. Like for N-N = dcbpy, the Ru-S coordination bond forms spontaneously in the dark and is cleaved by visible light irradiation.

DISCUSSION

Following previous work of Takeuchi,^{64,65} Rack,¹²⁻¹⁴ or Sauvage^{25,63} on the influence of steric hindrance on the photoreactivity of polypyridyl ruthenium(II) compounds we more recently realized²² that in the dark the Ru-S coordination bond of hindered complexes such as $[Ru(terpy)(dcbpy)(Hmte)]^{2+}$ spontaneously forms at room temperature and in neutral aqueous solutions, while still keeping a very high sensitivity to visible light irradiation. As dark formation and photochemical breakage can both occur, such systems open new possibilities for building supramolecular systems driven by visible light irradiation. However, the higher lability observed with the dcbpy complex seemed counterintuitive: for other light-sensitive complexes such as $[Ru(phen)_2(dmbpy)]^{2+}$ (phen = 1,10-phenanthroline, dmbpy = 6,6'-dimethyl-2,2'-bipyridine), steric hindrance leads to efficient photosubstitution²⁵ indeed, but also to a difficult thermal binding of the hindered chelate to the Ru center. The present study was undertaken to understand the relationship between thermal lability and steric hindrance for ruthenium complexes of the $[Ru(terpy)(N-N)(Hmte)]^{2+}$ family, and to gather temperature-dependent kinetic data that had been overlooked in the past.

First, it might be noticed that the substituents in *ortho* position to the coordinated nitrogen atoms of N-N = biq, dcbpy, and dmbpy do not only increase the steric bulk of the coordination sphere around the metal, but they also exert electronic effect on the metal center, which may in turn

Scheme 3. Proposed Transition States for the Substitution of the Aqua Ligand in $[Ru(terpy)(N-N)(H_2O)]^{2+}$ by Hmte, Where (a) N-N = bpy, biq^a and (b) N-N = dcbpy, dmbpy^b



^aMore compact transition state with hydrogen-bonding contributing to a loose hepta-coordinated transition state.

^bLess compact transition state.

influence the rates of ligand substitutions. This effect can be seen for example on the absorption maximum of the RuHmte complexes $[5]^{2+}$ – $[8]^{2+}$, which lies at significant higher wavelength for N–N = biq ($\lambda_{\max} = 519$ nm) than for N–N = bpy, dc bpy, or dmbpy ($\lambda_{\max} = 450, 467,$ and 463 nm, respectively). These electronic effects might play a role in fine-tuning the activation enthalpies and entropies of the thermal substitution reactions. However, one substituent of the bidentate chelate and the monodentate ligand coordinated to the metal center lie in very close spatial proximity, thus leading to significant distortion of the geometry in the ground state (compare for example the X-ray structures of $[5]^{2+}$ and $[7]^{2+}$). Thus, in the following discussion we mostly interpret the change in mechanism along the series bpy, biq, dc bpy, dmbpy as a consequence of the increasing steric demands of the spectator diimine chelate.

Usually, the higher thermal lability for sterically hindered complexes is explained in terms of destabilization of the ground-state hexacoordinated species, compared to the transition state of the thermal substitution reaction. In such interpretation, the reaction always follows a dissociative interchange mechanism.^{64,69–72} Applied to our system, this explanation should lead to enthalpy (ΔH_i^\ddagger) being the main reason for the decreased activation Gibbs energies (ΔG_i^\ddagger) when going from N–N = bpy to N–N = dmbpy. However, our data suggest that the increased lability of the hindered complexes in water is due to variations of the entropic term (ΔS_i^\ddagger) in Eyring's equation. Although ΔS_i^\ddagger values are known to contain significant experimental error and may be less accurate than, for example, activation volumes ΔV_i^\ddagger , the similarities in ΔH_i^\ddagger for the four systems and the clear differences in ΔS_i^\ddagger , as seen in Figure 7, allow drawing some mechanistic conclusions. Considering that for all four systems the rate law is first order in Hmte we conclude that there is a shift in the mechanism of the thermal substitution of H₂O by Hmte, from interchange associative with N–N = bpy and biq, marked by $\Delta S_i^\ddagger < 0$, to interchange dissociative with N–N = dc bpy and dmbpy, marked by $\Delta S_i^\ddagger > 0$.^{73–82} As shown in Scheme 3, H₂O is still present in the coordination sphere when the Ru–S bond-making occurs, and in an interchange mechanism bond making occurs before the second coordination sphere has had time to relax. For less bulkier chelates (N–N = bpy, biq) the Ru–S bond-making is essentially synchronous with the Ru–O bond-breaking (I_a mechanism). Hydrogen bonding between Hmte and the aqua ligand may also contribute to stabilizing the hepta-coordinated transition state. Thus, a more compact transition state and more constraints for the unhindered chelates N–N = bpy and biq lead to negative values for the activation entropy, and thus to significantly (bpy) or slightly (biq) lower substitution rate constants. In contrast, for bulkier systems the Ru–S bond making only occurs when Ru–OH₂ is already partially broken, but before H₂O exits from the second coordination sphere (I_d mechanism). Thus, there is no formation of a coordinatively unsaturated and potentially highly reactive pentacoordinated state, which would cancel the dependence of the substitution rate law in [Hmte]. The less compact transition state for N–N = dc bpy and dmbpy increases the degrees of freedom of both incoming and leaving monodentate ligands, thus resulting in positive activation entropies for the substitution process, which significantly enhances its rate constants.^{65,69,77,82–87}

CONCLUSION

The thermodynamic, kinetic, and photochemical properties of a series of polypyridyl ruthenium complexes $[\text{Ru}(\text{terpy})(\text{N}-\text{N})(\text{L})]^{2+}$ where N–N is bpy, biq, dc bpy, or dmbpy, and L is H₂O or Hmte, have been determined in water near neutral pH. Our data provide a global understanding of the influence of the N–N chelate on the reactivity of these systems. Qualitatively, a global acceleration of all thermal and photochemical ligand exchange processes is observed when the steric hindrance of the spectator diimine chelate is increased. Variable-temperature kinetic data show that the increased lability of the monodentate ligand with hindered N–N chelates is due to entropy, and that the mechanism of the thermal ligand substitution reaction changes from interchange associative to interchange dissociative following the series N–N = bpy, biq, dc bpy, dmbpy. Analysis of the relative values of the rate constants for the thermal and photochemical ligand substitution reactions also shows that by increasing the steric hindrance too much (N–N = dmbpy) the lability in the dark becomes so high that no appreciable change of the composition of the solution can be obtained by light irradiation, unless exceptionally intense light would be used. With intermediate steric hindrance (N–N = biq or dc bpy) the Ru–S bond forms spontaneously in the dark at room temperature, but it is efficiently cleaved under mild irradiation, which will allow using these systems in supramolecular chemistry. With the nonhindered ligand N–N = bpy, the photosensitivity of the Hmte complex is lower, and the monodentate ligands (Hmte and H₂O) are nonlabile at room temperature. Overall, changing the N–N bidentate ligand appears as an efficient means to tune the thermal and photochemical reactivities of $[\text{Ru}(\text{terpy})(\text{N}-\text{N})\text{L}]^{2+}$ complexes.

EXPERIMENTAL SECTION

Synthesis. ¹H and ¹³C NMR spectra were recorded using a Bruker DPX-300 spectrometer; chemical shifts are indicated in ppm relative to TMS. Electrospray mass spectra were recorded on a Finnigan TSO-quantum instrument using an electrospray ionization technique (ESI-MS). UV–vis spectra were obtained on a Perkin-Elmer Lambda 900 spectrophotometer or on a Varian Cary 50 UV–visible spectrometer. The classical routes for synthesizing $[\text{Ru}(\text{terpy})(\text{biq})(\text{Cl})] \text{Cl}$ ([10]-Cl),⁶⁴ $[\text{Ru}(\text{terpy})(\text{dmbpy})(\text{Cl})] \text{Cl}$ ([12]-Cl), and $[\text{Ru}(\text{terpy})(\text{dc bpy})(\text{Cl})] \text{Cl}$ ([11]-Cl),⁶⁷ were modified (see Supporting Information). $[\text{Ru}(\text{terpy})\text{Cl}_3]$,⁸⁸ 6,6-dichloro-2,2'-bipyridine,⁸⁹ $[\text{Ru}(\text{terpy})(\text{bpy})(\text{Cl})] \text{Cl}$ ([9]-Cl), $[\text{Ru}(\text{terpy})(\text{bpy})(\text{OH}_2)](\text{PF}_6)_2$ ([1](PF₆)₂),^{33,68} and $[\text{Ru}(\text{terpy})(\text{dc bpy})(\text{Hmte})](\text{PF}_6)_2$ ([7](PF₆)₂),²² were synthesized following literature procedures. 2,2';6',2''-terpyridine was purchased from ABCR GmbH & Co.KG. 2,2'-bipyridine, 6,6'-dimethyl-2,2'-bipyridine, 2,2'-biquinoline, 2-(methylthio)-ethanol (Hmte), and AgPF₆ were purchased from Sigma-Aldrich and used as such.

$[\text{Ru}(\text{terpy})(\text{bpy})(\text{Hmte})](\text{PF}_6)_2$ ([5](PF₆)₂). [9]Cl (56 mg, 0.10 mmol) and AgPF₆ (57 mg, 0.22 mmol) were dissolved in 3:5 acetone/H₂O mixture (16 mL). To this solution was added Hmte (90 μL, 1.0 mmol). The mixture was refluxed under argon for 8 h in the absence of light, after which it was filtered hot over *Celite*. Evaporation of the filtrate gave an orange solid, which was taken up in acetone and reprecipitated with Et₂O. Filtration of the suspension yielded [5](PF₆)₂ as an orange powder (69 mg, 79%). ¹H NMR (300 MHz, Acetone, 297 K, see Supporting Information, Figure S2) δ 9.95 (d, J = 5.6 Hz, 1H, A6), 9.03–8.87 (m, 3H, A3+T3'), 8.78 (d, J = 8.1 Hz, 2H, T3), 8.72 (d, J = 8.2 Hz, 1H, B3), 8.59–8.42 (m, 2H, A4+T4'), 8.26–8.09 (m, 3H, A5+T4), 8.09–7.94 (m, 3H, B4+T6), 7.63–7.47 (m, 3H, B6+T5), 7.31 (t, J = 6.6 Hz, B6, B5), 3.55 (t, J = 5.5 Hz, 2H, S-CH₂-CH₂), 2.03–1.97 (m, 2H, S-CH₂), 1.53 (s, 3H, S-Me). ¹³C NMR (75 MHz, Acetone, 297 K) δ 158.48 + 157.94 + 157.23 + 157.18

(B2+A2+T2+T2'), 153.89 (T6), 152.61 (A6), 150.56 (B6), 139.34 (T4), 138.67 + 138.58 (B4+A4), 137.42 (T4'), 129.03 (T5), 128.37 (A5), 127.71 (B5), 125.45 (T3), 125.16 (A3), 124.76 (T3'), 124.30 (B4), 58.37 (S-CH₂-CH₂), 37.17 (S-CH₂), 14.38 (S-Me). UV-vis: λ_{max} (ϵ in L·mol⁻¹·cm⁻¹) in pure H₂O: 450 nm (6600). ES MS *m/z* (*calc*): 728.0 (727.7 [M - PF₆]⁺), 582.1 (581.7 [M - 2 PF₆ - H]⁺), 261.5 (261.3 [M - 2PF₆ - Hmte + MeOH]²⁺). Anal. Calcd for C₂₈H₂₇F₁₂N₃OP₂RuS: C, 38.54; H, 3.12; N, 8.03; S, 3.67. Found: C, 38.25; H, 3.41; N, 7.94; S, 3.78. *Crystal growing*: Large single crystals of compound [5](PF₆)₂ were grown by vapor diffusion of toluene into a solution of [1](PF₆)₂ in Hmte (~10 mg in 0.5 mL mte). *Crystal structure data*: [C₂₈H₂₇N₃ORuS](PF₆)₂; Fw = 872.62, red block, 0.45 × 0.25 × 0.24 mm³, monoclinic, C2/c (no. 15), *a* = 24.06815(17), *b* = 10.86063(8), *c* = 24.69614(19) Å, β = 93.6407(7)°, *V* = 6442.43(8) Å³, *Z* = 8, *D_x* = 1.799 g cm⁻³, μ = 0.755 mm⁻¹, abs. corr. range: 0.769–0.867. 31610 Reflections were measured up to a resolution of (sin θ / λ)_{max} = 0.65 Å⁻¹. A total of 5673 reflections were unique (*R*_{int} = 0.0367), of which 5375 were observed [*I* > 2σ(*I*)]. 511 Parameters were refined with 195 restraints. *R*₁/*wR*₂ [*I* > 2σ(*I*)]: 0.0207/0.0517. *R*₁/*wR*₂ [all refl.]: 0.0226/0.0525. *S* = 1.051. Residual electron density found between -0.55 and 0.37 eÅ⁻³.

[Ru(*terpy*)(*biq*)(*Hmte*)²⁺] (**6**)²⁺. [10]Cl (4.0 mg, 6.0 μmol) was dissolved in D₂O (0.50 mL). To this solution a large excess of Hmte (50 μL, 0.51 mmol) was added and stirred for 5 min. The mixture was kept for 3 h at 80 °C in a water bath. According to ¹H NMR and ES MS, [6]²⁺ is the only ruthenium species in solution. (For atom numbering see Supporting Information, Figure S1) ¹H NMR (300 MHz, D₂O, 297 K) δ 8.97 (dd, *J* = 19.4, 8.8 Hz, 2H, B3+B4), 8.66 (d, *J* = 8.2 Hz, 4H, B8+T3'+A3), 8.47 (d, *J* = 8.0 Hz, 2H, T3), 8.43–8.33 (m, 3H, B5+A4+T4'), 8.14–7.92 (m, 6H, T4+B6+B7+T6), 7.85 (d, *J* = 7.4 Hz, 1H, A5), 7.55–7.40 (m, 3H, T5+A6), 7.25 (t, *J* = 7.9 Hz, 1H, A7), 6.50 (d, *J* = 8.8 Hz, 1H, A8), 3.30 (t, *J* = 7.1, 4.4 Hz, 2H, S-CH₂-CH₂), 1.54 (t, *J* = 5.8 Hz, 2H, S-CH₂-CH₂), 1.03 (s, 3H, CH₃-S). ¹³C NMR (75 MHz, D₂O, 297 K) δ 159.83 + 159.80 (T2+T2'), 158.17 + 158.00 (A2+B2), 153.46 (T6), 150.19 + 149.91 (A8a+B8a), 140.32 + 139.36 (B8+A8), 139.46 (T4), 137.94 (T4'), 133.09 (B6+A6), 130.60 + 130.05 (A7+B7), 129.75 + 128.80 (B4a+ A4a), 129.64 + 129.04 (A4+B4), 128.76 (T5), 126.92 + 123.06 (B5+A5), 125.03 + 124.34 (T3+T3'), 121.24 + 120.87 (A3+B3), 57.32 (S-CH₂-CH₂), 46.78 (S-CH₂-CH₂), 8.48 (CH₃-S). UV-vis (see Supporting Information): λ_{max} (ϵ in L·mol⁻¹·cm⁻¹) in pure H₂O: 519 nm (5600). ES MS *m/z* (*calc*): 682.0 (682.1 [M - 2Cl-H]⁺), 295.5 (295.3 [M - 2Cl-Hmte]²⁺).

[Ru(*terpy*)(*dmbpy*)(*Hmte*)²⁺] (**8**)²⁺. [12]Cl (4.0 mg, 6.8 μmol) was dissolved in D₂O (0.50 mL). To this solution a large excess of Hmte (24 μL, 0.28 mmol) was added. The mixture was stirred for 5 min. The compound was not isolated as it would react back to [12]Cl upon evaporation of water. According to ¹H NMR and MS [8]²⁺ is the only ruthenium species present in solution. (For atom notations see Supporting Information, Figure S1) ¹H NMR (300 MHz, D₂O, 297 K) δ 8.57 (d, *J* = 8.2 Hz, 2H, T3'), 8.45 (d, *J* = 8.0 Hz, 3H, B3+T3), 8.26 (t, *J* = 8.1 Hz, 1H, T4'), 8.21–8.01 (m, 6H, B4+A3+T4+T6), 7.81 (d, *J* = 7.6 Hz, 1H, B5), 7.61 (t, *J* = 7.9 Hz, 1H, A4), 7.55–7.46 (m, 2H, T5), 6.88 (d, *J* = 7.6 Hz, 1H, A5), 3.26 (t, *J* = 5.7 Hz, 2H, S-CH₂-CH₂), 3.09 (s, 3H, H7), 1.39 (t, *J* = 5.6 Hz, 2H, S-CH₂), 1.27 (s, 3H, H7'), 0.87 (s, 3H, S-Me). ¹³C NMR (300 MHz, D₂O) δ 165.61 + 164.45 (B6+A6), 158.94 + 158.38 (T2+T2'), 158.12 + 158.06 (B2+A2), 153.82 (T6), 138.99 (T4), 138.33 (A4), 138.15 (B4), 136.95 (T4'), 128.58 (T5), 127.76 (A5), 127.32 (B5), 124.61 (T3), 123.77 (T3'), 121.80 (A3), 121.38 (B3), 56.46 (HO-CH₂-), 34.71 (Me-S-CH₂-), 26.86 (A7), 22.00 (B7), 11.70 (Me-S). UV-vis (see Supporting Information): λ_{max} (ϵ in L·mol⁻¹·cm⁻¹) in pure H₂O: 463 nm (5700). ES MS *m/z* (*calc*): 610.1 (609.8 [M - 2Cl - H]⁺), 305.6 (305.3 [M - 2Cl]²⁺).

*General Procedure for the Hydrolysis in CD₃OD of [Ru(*terpy*)(*N*-*N*)(Cl)]Cl ([10]Cl, [11]Cl, or [12]Cl, *N*-*N* = *biq*, *dcbpy*, or *dmbpy*)*. Three NMR samples of compound [10]Cl (2.2 mg, 3.3 × 10⁻³ mmol), [11]Cl (2.8 mg, 4.8 × 10⁻³ mmol), or [12]Cl (2.9 mg, 4.6 × 10⁻³ mmol) were dissolved in MeOD (500 μL). An ¹H NMR spectrum was recorded for each sample. Then, 20 μL, 40 μL, 80 μL,

and 160 μL of D₂O were added successively to each NMR tube, and ¹H NMR spectra were recorded after each addition (see Supporting Information, Figure S4).

Equilibrium Constant Determination. (a) For *N*-*N* = *biq* ([2]Cl₂ ⇌ [6]Cl₂): A stock solution A of [10]Cl (17 mg in 5.0 mL D₂O, 5.1 mM) and a stock solution B of Hmte (92 mg Hmte in 2.0 mL D₂O, 0.50 M) were prepared. Eight NMR tubes containing 0.50 mL of solution A (2.5 μmol [10]Cl) were prepared, and to each tube was added 2.5 μL, 5.0 μL, 8.0 μL, 10 μL, 15 μL, 26 μL, 34 μL, or 35 μL solution B, resulting in 0.50, 1.0, 1.6, 2.0, 3.0, 5.2, 6.8, or 7.0 equivalents of Hmte, respectively. The NMR tubes were put in a water bath for 30 min at 50 °C and left standing overnight at room temperature. After equilibration, ¹H NMR spectra of all samples were measured at room temperature, to determine the relative integral of [6]²⁺ and [2]²⁺. Then the ratios [RuHmte]/[RuOH₂] were determined by integration of the peaks at 6.35 and 6.75 ppm corresponding to [6]²⁺ and [2]²⁺, respectively, where [RuHmte] represents the concentration in [6]²⁺ and [RuOH₂] the concentration in [2]²⁺. A plot of [RuHmte]/[RuOH₂] as a function of equilibrium concentration in Hmte was made. The slope of the plot numerically corresponds to *K*₂ (see Figure 4 and eq 1).

(b) For *N*-*N* = *dmbpy* ([4]Cl₂ ⇌ [8]Cl₂): A stock solution C of [12]Cl (40 mg in 5.0 mL D₂O, 13 mM) was prepared. NMR samples, each containing 0.50 mL of stock solution C (6.4 μmol [12]Cl) were prepared. To each NMR tube was added a known amount of pure Hmte (0.60 μL, 1.2 μL, 1.8 μL, 2.4 μL, 3.0 μL, 4.5 or 6.0 μL) to give 1.0, 2.0, 3.0, 4.0, 5.0, 7.5, 10, or 20 equivalents, respectively. Each NMR tube was stirred for 5 min and then left to stand for more than 10 min at room temperature. After equilibration, ¹H NMR spectra of all samples were measured at room temperature. The ratio [RuHmte]/[RuOH₂] were determined by integration of the peaks at 6.86 and 6.78 ppm, where [RuHmte] represents the concentration in [8]²⁺ (δ = 6.86 ppm) and [RuOH₂] the concentration in [4]²⁺ (δ = 6.78 ppm). A plot of [RuHmte]/[RuOH₂] as a function of equilibrium concentration in Hmte was made. The slope of the plot numerically corresponds to *K*₄ (see Figure 4 and eq 1).

The values for Gibbs free energy ΔG° , at 297 K were calculated for both reactions using the equation $\Delta G^\circ = -RT \ln K$.

Kinetics. A Perkin-Elmer Lambda 900 UV-vis spectrometer equipped with stirring and temperature control was used for kinetic experiments. The measurement procedure and values of the extinction coefficients of all aqua and Hmte complexes used in the kinetic study is described in the Supporting Information, Figure S6 and Table S1. The experimental procedure for the calculation of the rate constants at 297 K from the slope of a plot of *k*'_i vs [Hmte] is explained in the Supporting Information.

Thermal Substitution of H₂O by Hmte on RuOH₂ Complexes (*k*_i, ΔH^\ddagger , ΔS^\ddagger , ΔG^\ddagger). Stock solutions D of complex [1](PF₆)₂ (2.0 mg in 25 mL of H₂O, 1.0 × 10⁻⁴ M), E of [10]Cl (1.6 mg in 25 mL of H₂O, 1.0 × 10⁻⁴ M), F of [11]Cl (3.7 mg in 25 mL of H₂O, 2.1 × 10⁻⁴ M), G of [12]Cl (3.5 mg in 25 mL of H₂O, 2.2 × 10⁻⁴ M), and H and I of Hmte (460 mg in 25.0 mL of H₂O, 2.00 × 10⁻¹ M (H), and 438 mg in 10.0 mL of H₂O, 4.70 × 10⁻¹ M (I)) were prepared. 2.0 mL of D, E, F, or G was added to a UV-vis cuvette, which was placed in the UV-vis spectrometer. The temperature was set at 50, 60, 70, or 80 °C for D, 24, 28, 35, 42, or 50 °C for E, and 10, 15, 20, 24, or 28 °C for F and G. After obtaining a constant temperature in each cuvette, 1.0 mL of H was added to D and E, or 1 mL of I to F, or 0.8 mL of H₂O plus 0.2 mL of I to G, for each experiment at each temperature (final Hmte and Ru concentrations for each experiments are given in Supporting Information, Tables S2 and S3). In such conditions, Hmte is in large excess (pseudo first-order condition). After addition of Hmte, a UV-vis spectrum was taken every 60 s for D and every 30 s for E, F, or G. For each spectrum, the concentrations in [RuHmte] and [RuOH₂] were determined by deconvolution of the UV-vis spectra knowing the extinction coefficients of both RuHmte and RuOH₂ species (see Supporting Information and Table S1). The pseudo first order rate constants *k*'_i at each temperature for each sample D, E, F, or G were determined from the slope of the plot of ln([RuOH₂]/[Ru]_{tot}) vs time, and *k*_i were then calculated knowing the

concentration of Hmte in the solution (see Supporting Information, Tables S2 and S3). By plotting $\ln(k_i/T)$ as a function of $1/T$ for each sample, the activation enthalpy and entropy were calculated from the slope and y -intercept of the Eyring plot, respectively. ΔG_i^\ddagger at 297 K was calculated for each reaction using the equation $\Delta G_i^\ddagger = \Delta H_i^\ddagger - T \times \Delta S_i^\ddagger$ (see Table 3).

Thermal Substitution of Hmte by H₂O in [5]²⁺ (k_{-1}). Three milliliters of a solution of [5]²⁺ (5.6 mg of [5](PF₆)₂ in 25 mL of H₂O, 2.5×10^{-4} M) was placed in a UV-vis cuvette, which was placed at $t = 0$ in the UV-vis spectrometer pre-equilibrated at 70, 75, 80, 85, or 90 °C. UV-vis spectra were measured every 60 s. The concentrations in [RuHmte] and [RuOH₂] were determined by deconvolution of the UV-vis spectra knowing the extinction coefficients of both RuHmte and RuOH₂ species (see Supporting Information and Table S1). The first-order rate constant k_{-1} at each temperature was determined by plotting $\ln([RuOH_2]/[Ru]_{tot})$ vs time. The slope and y -intercept of an Eyring plot afforded the activation enthalpy and entropy, respectively (see Supporting Information, Figure S10). k_{-1} at 24 °C was extracted from extrapolating the Eyring equation down to room temperature; a value of $1.5(4) \times 10^{-8}$ s⁻¹ was found.

Thermal Substitution of Hmte by H₂O on [6]²⁺, [7]²⁺, and [8]²⁺ (k_{-2} , k_{-3} , k_{-4}). At the thermodynamic equilibrium between RuOH₂, free Hmte, and RuHmte in water, the rates for the formation and hydrolysis of RuHmte complex are equal.

$$k_{-i} \cdot [RuHmte]_{eq} = k_i \cdot [RuOH_2]_{eq} \cdot [Hmte]_{eq}$$

Thus the first-order rate constant k_{-i} for the thermal substitution free Hmte by water is numerically given by $k_{-i} = k_i/K$. The activation Gibbs energy ΔG_{-i}^\ddagger for the thermal substitution of Hmte by H₂O were calculated using the equation $\Delta G_{-i}^\ddagger = \Delta G_i^\ddagger - \Delta G_i^\circ$ (see Table 3).

Photochemistry. The photochemical quantum yield for [5]²⁺ was measured using a Varian Cary 50 UV-visible spectrometer and a LOT 1000 W xenon arc lamp, fitted with a water filter and a 450FS10-50 Andover interference filter ($\lambda_e = 452$ nm, $\Delta\lambda_{1/2} = 8.9$ nm). Irradiation was thus performed close to the isosbestic point of the reaction, which was at 449 nm. The photochemistry measurements for [6]²⁺, [7]²⁺, and [8]²⁺ were done using a Perkin-Elmer Lambda 900 spectrometer equipped with a custom-made LED lamp fitted to the top of a 1 cm quartz UV-vis cuvette, using an OSRAM Opto electronics LEDs LB WSKM-EZGY-35 ($\lambda_e = 465$ nm or $\lambda_e = 520$ nm, $\Delta\lambda_{1/2} = 25$ nm). In these cases, UV-vis measurements of a sample during irradiation was superimposable with a spectrum of the sample when the LED lamp was switched off, which means that the light used to irradiate the sample perpendicularly to the optical axis of the spectrophotometer was not detected by the spectrometer. Photon fluxes of the three irradiation setups were measured using the ferrioxalate actinometer;⁹⁰ a value $\Phi = 6.4(6) \times 10^{-8}$ Einstein s⁻¹ was measured at 452 nm for the filtered LOT lamp; $\Phi = 3.9(4) \times 10^{-9}$ Einstein s⁻¹ was found for the LED at 465 nm, and $\Phi = 9.8(8) \times 10^{-10}$ Einstein s⁻¹ was found for the LED at 520 nm. In the latter two cases, the irradiation path length was 3 cm, and the volume of the irradiated solution was 3 mL.

Photosubstitution Quantum Yield Determination for Complex [5]²⁺ (ϕ_1). 0.75 mL of a stock solution of the complex [5](PF₆)₂ (5.0 mg in 10 mL of H₂O, 5.7×10^{-4} M) was put in a UV-vis cuvette. The volume of the solution was completed to 3 mL with H₂O (Final concentration: 1.5×10^{-4} M). The sample was irradiated using the same setup as was used for actinometry ($\Phi = 6.4(6) \times 10^{-8}$ Einstein s⁻¹). After each irradiation period (1 min) a UV-vis spectrum was measured until a total irradiation time of 10 min. The concentrations in [5]²⁺ and [1]²⁺ were determined by deconvolution knowing the extinction coefficients of both species (see Supporting Information and Table S1). The evolution of $\ln([RuHmte]/[Ru]_{tot})$ was plotted as a function of irradiation time, and from the slope S of the plot and using Equation 11, the quantum yield ϕ_1 was determined to be 0.022(6) (see Supporting Information, Table S5).

Irradiation of an Equilibrated Sample of the Big System ([2]Cl₂ ⇌ [6]Cl₂) and Photosubstitution Quantum Yield Determination for [6]²⁺ (ϕ_2). A UV-vis cuvette containing 2 mL of a stock solution of [10]Cl (1.5 mg in 10 mL of H₂O, 2.3×10^{-4} M) and

1 mL of a solution of Hmte (31 mg in 10 mL of H₂O, 0.030 M) was prepared and stirred overnight to reach equilibrium at 24 °C. Then, UV-vis spectra were measured, once in the dark, and then during 45 min under irradiation using LED lamp at $\lambda_e = 520$ nm. After 45 min the LED lamp was switched off, and UV-vis spectra were measured for 90 min in the dark (1 min interval between each spectrum, either under irradiation or in the dark). The cycle was repeated 3 more times for a total experimental time of 9 h (see Figure 8). For each spectrum [RuHmte] and [RuOH₂], that is, the concentration in [6]²⁺ and [2]²⁺, respectively, were determined by deconvolution, knowing the extinction coefficients of both species (see Supporting Information, Table S1). By calculating the ratio [RuHmte]/[RuOH₂] at the equilibrium in the dark (eq 8a) and at the photochemical steady state (eq 8b), reporting the second order rate constant k_2 and the photon flux ϕ , the quantum yield ϕ_2 was calculated using eq 9, to be 0.12(5) (see Supporting Information, Table S5 for all numerical values).

Determination of the Photosubstitution Quantum Yield for [8]²⁺ (ϕ_4). 2.0 mL of a stock solution of [8]Cl (7.0 mg in 50 mL H₂O, 2.2×10^{-4} M) was put in a UV-vis cuvette and 1 mL of a solution of Hmte (277 mg in 5.00 mL of H₂O, 0.600 M) was added. After equilibration at 24 °C in the dark, UV-vis spectra of the sample were measured in the dark and then 10 times during 10 min irradiation with an LED lamp at $\lambda_e = 465$ nm to calculate ϕ_4 in the same procedure as that for [6]²⁺. A value of 0.30(6) was found for ϕ_4 (see Supporting Information, Table S5).

■ ASSOCIATED CONTENT

● Supporting Information

The synthesis of [10]Cl, [12]Cl, proton attribution schemes, ¹H NMR spectra in D₂O and MeOD/D₂O mixtures, procedure for X-ray crystal structure determination, extinction coefficient determination procedure and values, mathematical modeling of the fast equilibrium between [4]²⁺ and [8]²⁺, numerical values of first-order and second-order rate constant for all four systems, determination of the rate law (order of Hmte) of the thermal coordination reaction for N–N = bpy, biq, and dmbpy, Eyring plot for the thermal hydrolysis of [5]²⁺, pK_a measurements for [2]²⁺ and [4]²⁺, and photosubstitution quantum yield measurements. This material is available free of charge via the Internet at <http://pubs.acs.org>.

■ AUTHOR INFORMATION

Corresponding Author

*E-mail: bonnet@chem.leidenuniv.nl

Notes

The authors declare no competing financial interest.

■ ACKNOWLEDGMENTS

Leiden University is kindly acknowledged for financial support. The Dutch Organization for Scientific Research (NWO–CW/Vernieuwingsimpuls) is kindly acknowledged for a Veni grant to S.B.

■ REFERENCES

- (1) Ryabov, A. D.; Kuzmina, L. G.; Dvortsova, N. V.; Stufkens, D. J.; van Eldik, R. *Inorg. Chem.* **1993**, *32*, 3166.
- (2) Nishihara, H. *Coord. Chem. Rev.* **2005**, *249*, 1468.
- (3) Wenger, O. S.; Henling, L. M.; Day, M. W.; Winkler, J. R.; Gray, H. B. *Polyhedron* **2004**, *23*, 2955.
- (4) Han, M.; Hirade, T.; Hara, M. *New J. Chem.* **2010**, *34*, 2887.
- (5) Pratihar, P.; Mondal, T. K.; Patra, A. K.; Sinha, C. *Inorg. Chem.* **2009**, *48*, 2760.
- (6) Mitsuoka, T.; Sato, H.; Yoshida, J.; Yamagishi, A.; Einaga, Y. *Chem. Mater.* **2006**, *18*, 3442.
- (7) Kopelman, R. A.; Snyder, S. M.; Frank, N. L. *J. Am. Chem. Soc.* **2003**, *125*, 13684.

- (8) Bannwarth, A.; Schmidt, S. O.; Peters, G.; Sönnichsen, F. D.; Thimm, W.; Herges, R.; Tuczek, F. *Eur. J. Inorg. Chem.* **2012**, 2012, 2776.
- (9) Takahashi, K.; Hasegawa, Y.; Sakamoto, R.; Nishikawa, M.; Kume, S.; Nishibori, E.; Nishihara, H. *Inorg. Chem.* **2012**, 51, 5188.
- (10) Segarra-Maset, M. D.; van Leeuwen, P. W. N. M.; Freixa, Z. *Eur. J. Inorg. Chem.* **2010**, 2075.
- (11) Boillot, M. L.; Zarembowitch, J.; Sour, A. *Top. Curr. Chem.* **2004**, 234, 261.
- (12) Lutterman, D. A.; Rachford, A. A.; Rack, J. J.; Turro, C. *J. Phys. Chem. Lett.* **2010**, 1, 3371.
- (13) Rachford, A. A.; Petersen, J. L.; Rack, J. J. *Inorg. Chem.* **2006**, 45, 5953.
- (14) Rack, J. J.; Winkler, J. R.; Gray, H. B. *J. Am. Chem. Soc.* **2001**, 123, 2432.
- (15) Sauvage, J. P. *Chem. Commun.* **2005**, 1507.
- (16) Balzani, V.; Clemente-Leon, M.; Credi, A.; Ferrer, B.; Venturi, M.; Flood, A. H.; Stoddart, J. F. *Proc. Natl. Acad. Sci. U. S. A.* **2006**, 103, 1178.
- (17) Agrawal, U. C.; Nigam, H. L. *J. Indian Chem. Soc.* **2008**, 85, 677.
- (18) Campagna, S.; Puntoriero, F.; Nastasi, F.; Bergamini, G.; Balzani, V. *Photochem. Photophys. Coord. Compd. I* **2007**, 280, 117.
- (19) Balzani, V.; Credi, A.; Venturi, M. *Chem. Soc. Rev.* **2009**, 38, 1542.
- (20) Bonnet, S.; Collin, J. P.; Koizumi, M.; Mobian, P.; Sauvage, J. P. *Adv. Mater.* **2006**, 18, 1239.
- (21) Bonnet, S.; Collin, J.-P. *Chem. Soc. Rev.* **2008**, 37, 1207.
- (22) Bahreman, A.; Limburg, B.; Siegler, M. A.; Koning, R.; Koster, A. J.; Bonnet, S. *Chem.—Eur. J.* **2012**, 18, 10271.
- (23) Collin, J. P.; Heitz, V.; Bonnet, S.; Sauvage, J. P. *Inorg. Chem. Commun.* **2005**, 8, 1063.
- (24) Mobian, P.; Kern, J. M.; Sauvage, J. P. *Angew. Chem., Int. Ed.* **2004**, 43, 2392.
- (25) Laemmel, A. C.; Collin, J. P.; Sauvage, J. P. *Eur. J. Inorg. Chem.* **1999**, 383.
- (26) Bednarski, P. J.; Mackay, F. S.; Sadler, P. J. *Anti-Cancer Agents Med. Chem.* **2007**, 7, 75.
- (27) Farrer, N. J.; Salassa, L.; Sadler, P. J. *Dalton Trans.* **2009**, 10690.
- (28) Howerton, B. S.; Heidary, D. K.; Glazer, E. C. *J. Am. Chem. Soc.* **2012**, 134, 8324.
- (29) Wachter, E.; Heidary, D. K.; Howerton, B. S.; Parkin, S.; Glazer, E. C. *Chem. Commun.* **2012**, 48, 9649.
- (30) Indelli, M.; Chiorboli, C. *Top. Curr. Chem.* **2007**, 280, 215.
- (31) Mahnken, R. E.; Billadeau, M. A.; Nikonowicz, E. P.; Morrison, H. *J. Am. Chem. Soc.* **1992**, 114, 9253.
- (32) Schatzschneider, U.; Niesel, J.; Ott, I.; Gust, R.; Alborzina, H.; Woelfl, S. *ChemMedChem* **2008**, 3, 1104.
- (33) Goldbach, R. E.; Rodriguez-Garcia, I.; van Lenthe, J. H.; Siegler, M. A.; Bonnet, S. *Chem.—Eur. J.* **2011**, 17, 9924.
- (34) Moucheron, C.; KirschDeMesmaeker, A.; Kelly, J. J. *Photochem.* **1997**, 40, 91.
- (35) Higgins, S. L. H.; Brewer, K. J. *Angew. Chem., Int. Ed.* **2012**, 51, 2.
- (36) Garner, R. N.; Gallucci, J. C.; Dunbar, K. R.; Turro, C. *Inorg. Chem.* **2011**, 50, 9213.
- (37) De Candia, A. G.; Marcolongo, J. P.; Etchenique, R.; Slep, L. D. *Inorg. Chem.* **2010**, 100625124914047.
- (38) Zayat, L.; Calero, C.; Albores, P.; Baraldo, L.; Etchenique, R. *J. Am. Chem. Soc.* **2003**, 125, 882.
- (39) Fry, N. L.; Mascharak, P. K. *Acc. Chem. Res.* **2011**, 44, 289.
- (40) Rose, M. J.; Mascharak, P. K. *Coord. Chem. Rev.* **2008**, 252, 2093–2114.
- (41) Barragán, F.; López-Senín, P.; Salassa, L.; Betanzos-Lara, S.; Habtemariam, A.; Moreno, V.; Sadler, P. J.; Marchán, V. *J. Am. Chem. Soc.* **2011**, 133 (35), 14098–14108.
- (42) Salassa, L.; Garino, C.; Salassa, G.; Gobetto, R.; Nervi, C. *J. Am. Chem. Soc.* **2008**, 130, 9590.
- (43) Howerton, B. S.; Heidary, D. K.; Glazer, E. C. *J. Am. Chem. Soc.* **2012**, 134, 8324.
- (44) Respondek, T.; Garner, R. N.; Herroon, M. K.; Podgorski, I.; Turro, C.; Kodanko, J. J. *J. Am. Chem. Soc.* **2011**, 133, 17164.
- (45) Lutterman, D. A.; Fu, P. K. L.; Turro, C. *J. Am. Chem. Soc.* **2006**, 128, 738.
- (46) Balzani, V.; Bergamini, G.; Campagna, S.; Puntoriero, F. *Top. Curr. Chem.* **2007**, 280, 1.
- (47) Paris, J. P.; Brandt, W. W. *J. Am. Chem. Soc.* **1959**, 81, 5001.
- (48) Anderson, C. P.; Salmon, D. J.; Meyer, T. J.; Young, R. C. *J. Am. Chem. Soc.* **1977**, 99, 1980.
- (49) Van Houten, J.; Watts, R. J. *J. Am. Chem. Soc.* **1976**, 98, 4853.
- (50) Durham, B.; Caspar, J. V.; Nagle, J. K.; Meyer, T. J. *J. Am. Chem. Soc.* **1982**, 104, 4803.
- (51) Hecker, C. R.; Fanwick, P. E.; McMillin, D. R. *Inorg. Chem.* **1991**, 30, 659.
- (52) Baranoff, E.; Collin, J. P.; Furusho, Y.; Laemmel, A. C.; Sauvage, J. P. *Chem. Commun.* **2000**, 1935.
- (53) Durham, B.; Walsh, J. L.; Carter, C. L.; Meyer, T. J. *Inorg. Chem.* **1980**, 19, 860.
- (54) Bonnet, S.; Collin, J. P.; Gruber, N.; Sauvage, J. P.; Schofield, E. R. *Dalton Trans.* **2003**, 4654.
- (55) Ashton, P. R.; Ballardini, R.; Balzani, V.; Credi, A.; Dress, K. R.; Ishow, E.; Kleverlaan, C. J.; Kocian, O.; Preece, J. A.; Spencer, N.; Stoddart, J. F.; Venturi, M.; Wenger, S. *Chem.—Eur. J.* **2000**, 6, 3558.
- (56) Ashton, P. R.; Ballardini, R.; Balzani, V.; Constable, E. C.; Credi, A.; Kocian, O.; Langford, S. J.; Preece, J. A.; Prodi, L.; Schofield, E. R.; Spencer, N.; Stoddart, J. F.; Wenger, S. *Chem.—Eur. J.* **1998**, 4, 2413.
- (57) Baranoff, E.; Collin, J. P.; Furusho, J.; Furusho, Y.; Laemmel, A. C.; Sauvage, J. P. *Inorg. Chem.* **2002**, 41, 1215.
- (58) Mobian, P.; Kern, J. M.; Sauvage, J. P. *J. Am. Chem. Soc.* **2003**, 125, 2016.
- (59) Nguyen, T. D.; Leung, K. C. F.; Liong, M.; Liu, Y.; Stoddart, J. F.; Zink, J. I. *Adv. Funct. Mater.* **2007**, 17, 2101.
- (60) Collin, J. P.; Jouvenot, D.; Koizumi, M.; Sauvage, J. P. *Inorg. Chem.* **2005**, 44, 4693.
- (61) Bonnet, S.; Collin, J. P.; Sauvage, J. P. *Inorg. Chem.* **2006**, 45, 4024.
- (62) Gianferrara, T.; Bergamo, A.; Bratsos, I.; Milani, B.; Spagnul, C.; Sava, G.; Alessio, E. *J. Med. Chem.* **2010**, 53, 4678.
- (63) Bonnet, S.; Collin, J. P.; Sauvage, J. P.; Schofield, E. *Inorg. Chem.* **2004**, 43, 8346.
- (64) Bessel, C. A.; Margarucci, J. A.; Acquaye, J. H.; Rubino, R. S.; Crandall, J.; Jircitano, A. J.; Takeuchi, K. J. *Inorg. Chem.* **1993**, 32, 5779.
- (65) Leising, R. A.; Ohman, J. S.; Takeuchi, K. J. *Inorg. Chem.* **1988**, 27, 3804.
- (66) Wasylenko, D. J.; Ganesamoorthy, C.; Koivisto, B. D.; Henderson, M. A.; Berlinguette, C. P. *Inorg. Chem.* **2010**, 49, 2202.
- (67) Che, C. M.; Ho, C.; Lau, T. C. *J. Chem. Soc., Dalton Trans.* **1991**, 1901.
- (68) Takeuchi, K. J.; Thompson, M. S.; Pipes, D. W.; Meyer, T. J. *Inorg. Chem.* **1984**, 23, 1845.
- (69) Swaddle, T. W. *Coord. Chem. Rev.* **1974**, 14, 217.
- (70) Mahanti, B.; De, G. S. *Transition Met. Chem.* **1994**, 19, 201.
- (71) Aebischer, N.; Laurenczy, G.; Ludi, A.; Merbach, A. E. *Inorg. Chem.* **1993**, 32, 2810.
- (72) Aebischer, N.; Churlaud, R.; Dolci, L.; Frey, U.; Merbach, A. E. *Inorg. Chem.* **1998**, 37, 5915.
- (73) Rotzinger, F. P. *J. Phys. Chem. A* **2000**, 104, 8787.
- (74) Bunten, K. A.; Farrar, D. H.; Poe, A. J.; Lough, A. J. *Organometallics* **2000**, 19, 3674.
- (75) Czap, A.; Heinemann, F. W.; van Eldik, R. *Inorg. Chem.* **2004**, 43, 7832.
- (76) Gamasa, M. P.; Gimeno, J.; GonzalezBernardo, C.; MartinVaca, B. M.; Monti, D.; Bassetti, M. *Organometallics* **1996**, 15, 302.
- (77) Kojima, T.; Morimoto, T.; Sakamoto, T.; Miyazaki, S.; Fukuzumi, S. *Chem.—Eur. J.* **2008**, 14, 8904.
- (78) Rilak, A.; Petrovic, B.; Grguric-Sipka, S.; Tesic, Z.; Bugarcic, Z. D. *Polyhedron* **2011**, 30, 2339.
- (79) Goswami, A. M.; De, K. *Transition Met. Chem.* **2007**, 32, 419.

- (80) Shoukry, M. M.; Shehata, M. R.; Hamza, M. S. A.; van Eldik, R. *Dalton Trans.* **2005**, 3921.
- (81) Naik, R. M.; Singh, R.; Asthana, A. *Int. J. Chem. Kinet.* **2011**, *43*, 21.
- (82) Thiel, V.; Hendann, M.; Wannowius, K.-J.; Plenio, H. *J. Am. Chem. Soc.* **2012**, *134*, 1104.
- (83) Wilkins, R. G. In *Kinetics and Mechanism of Reactions of Transition Metal Complexes*, 2nd ed.; Wiley-VCH: Weinheim, Germany, 1991; p 199.
- (84) Langford, C. H.; Muir, W. R. *J. Am. Chem. Soc.* **1967**, *89*, 3141.
- (85) Mukherjee, A.; De, K. *Transition Met. Chem.* **2005**, *30*, 677.
- (86) Krishnan, R.; Schultz, R. H. *Organometallics* **2001**, *20*, 3314.
- (87) Wang, F.; Chen, H. M.; Parsons, S.; Oswald, L. D. H.; Davidson, J. E.; Sadler, P. J. *Chem.—Eur. J.* **2003**, *9*, 5810.
- (88) Leising, R. A.; Kubow, S. A.; Churchill, M. R.; Buttrey, L. A.; Ziller, J. W.; Takeuchi, K. J. *Inorg. Chem.* **1990**, *29*, 1306.
- (89) Constable, E. C.; Seddon, K. R. *Tetrahedron* **1983**, *39*, 291.
- (90) Calvert, J. G.; Pitts, J. N., *Photochemistry*; Wiley and Sons: New York, 1967; p 780.